Identification of Protective, Metabolite-producing Bacterial and Viral Consortia in Allogeneic Stem Cell Transplantation Patients

Erik Thiele Orberg (e.orberg@tum.de)
Technical University Munich https://orcid.org/0000-0003-1969-8261

Elisabeth Meedt

Andreas Hiergeist
Institute of Microbiology Regensburg

Jinling Xue
Institute of Virology, Helmholtz Zentrum Munich

Sakhila Ghimire
University Medical Center Regensburg

Melanie Tiefgraber
University Hospital Rechts der Isar of the Technical University of Munich

Sophia Göldel
University Hospital Rechts der Isar of the Technical University of Munich

Tina Eismann
University Hospital Rechts der Isar of the Technical University of Munich

Alix Schwarz
University Hospital Rechts der Isar of the Technical University of Munich

Sebastian Jarosch
Technical University of Munich https://orcid.org/0000-0002-2908-8590

Katja Steiger
Institute of Pathology, School of Medicine, Technical University of Munich; https://orcid.org/0000-0002-7269-5433

Michael Gigl
Bavarian Center for Biomolecular Mass Spectrometry, Technical University of Munich

Karin Kleigrewe
Bavarian Center for Biomolecular Mass Spectrometry, Technical University of Munich

Julius Fischer
Technical University Munich https://orcid.org/0000-0002-6951-3416

Klaus-Peter Janssen
Technical University of Munich https://orcid.org/0000-0002-4707-7887

Michael Quante

Internal Medicine II, University Medical Center Freiburg

Simon Heidegger

Technical University Munich https://orcid.org/0000-0001-6394-5130

Peter Herhaus

University Hospital Rechts der Isar of the Technical University of Munich

Mareike Verbeek

University Hospital Rechts der Isar of the Technical University of Munich

Jürgen Ruland

Technical University of Munich https://orcid.org/0000-0002-8381-3597

Daniela Weber

University Medical Center Regensburg

Daniel Wolff

University Hospital Regensburg https://orcid.org/0000-0001-7015-3190

Matthias Edinger

University Medical Center Regensburg

Dirk Busch

Technichal University of Munich https://orcid.org/0000-0001-8713-093X

Wolfgang Herr

University Hospital Regensburg

Florian Bassermann

Technical University of Munich (TUM)

André Gessner

Institute of Clinical Microbiology and Hygiene, University Hospital Regensburg, 93053 Regensburg,

Li Deng

Institute of Virology, School of Medicine, Helmholtz Center Munich, Technical University of Munich

Ernst Holler

University Medical Centre, Regensburg

Hendrik Poeck

Universitiy of Regensburg

Article

Keywords:

Posted Date: April 14th, 2022

DOI: https://doi.org/10.21203/rs.3.rs-1504704/v1

Additional Declarations: Yes there is potential Competing Interest. Ernst Holler: Advisory Boards: Maat Pharma, Pharmabiome, Medac, Novartis, Neovii. Hendrik Poeck: Advisory Board: Gilead, Abbvie; Pfizer; Speaker/Consultants: Abbvie, Gilead, Novartis, Servier, Bristol Myers-Squibb, Pfizer; Funding: Bristol Myers-Squibb.

Version of Record: A version of this preprint was published at Nature Cancer on January 3rd, 2024. See the published version at https://doi.org/10.1038/s43018-023-00669-x.

Abstract

The intestinal bacteriome directly affects outcome in patients undergoing allogeneic hematopoietic stem cell transplantation (allo-SCT). Besides bacteria, fungal and viral communities as well as microbiota-derived metabolites play a role. Yet, it is still unclear how dynamic shifts in these three communities contribute to (1) clinical outcome of allo-SCT patients, (2) production of metabolites and (3) how they are affected by microbiome modulation via antibiotics or fecal microbiota transplantation (FMT). Here, we performed a prospective, longitudinal study that combined transkingdom (bacteria, fungi, viruses) analysis of intestinal microbial communities with targeted metabolomics in allo-SCT patients (n=78) at two different transplantation centers. We uncovered a microbiome signature of metabolite-producing bacteria from the Lachnospiraceae and Oscillospiraceae families and their corresponding bacteriophages, which correlated with the production of immunomodulatory metabolites including short-chain fatty acids (SCFAs), metabolites associated with induction of type-I IFN signaling (IIMs) and bile acids. Sustained production of these “protective” metabolites after allo-SCT was associated with improved survival and reduced transplantation-related mortality, whereas antibiotic exposure significantly impaired metabolite expression. We demonstrate that single taxa domination and metabolite depletion in a patient suffering from graft versus host disease (GvHD) could be rescued by transfer of metabolite-producing bacterial consortia via fecal microbiota transplantation (FMT). FMT led to resolution of steroid refractory GvHD and was accompanied by an increase of bacterial and viral alpha diversity, restoration of SCFAs and IIMs and accumulation of regulatory T cells to the intestine. Our study demonstrates that microbiome modulation (via antibiotics or FMT) can affect the identified bacterial/bacteriophage network and their associated protective metabolites thereby determining clinical outcomes and provides a rationale for the development of engineered metabolite-producing consortia and defined metabolite combination drugs as novel microbiome-based therapies.

Introduction

Allogeneic hematopoietic stem cell transplantation (allo-SCT) is a curative treatment option for many hematological diseases. However, success is limited if patients develop acute graft-versus-host disease (GvHD), still the most common life-threatening complication.[1] In patients undergoing allo-SCT, the intestinal bacterial microbiome is altered by loss of diversity and domination of disease-related taxa.[2–5] Multiple factors contribute to this GvHD-related microbial signature, such as use of antibiotics, administration of (radio-)chemotherapy and nutrition.[6,7] Alterations of bacterial communities strongly influence the pathophysiology of GvHD and affect outcome of patients undergoing allo-SCT.[8–12]

However, the impact of the virome and fungome on allo-SCT and GvHD is not as well studied. Furthermore, disruption of a single kingdom can have profound transkingdom effects. For example, loss of bacterial abundance can lead to an increase in viable fungi after allo-SCT and facilitate *Candida parapsilosis* complex species expansion, which is associated with increased transplantation-related mortality (TRM).[13] Although analyses of the human gut virome remain challenging due to the high degree

of viral-sequence diversity and continual discovery of novel viruses by metagenomics[14], a recent study of 44 allo-SCT patients linked picobirnaviruses to severe GI-GvHD.[15] How the dynamic shifts in these kingdoms and associated transkingdom effects contribute to clinical outcome, such as infection due to loss of colonization resistance[16], but also intestinal inflammation and tissue damage in GI-GvHD needs to be further investigated.[15]

Recently, microbiota-derived metabolites such as short-chain fatty acids (SCFAs), tryptophan derivates such as indoles and secondary bile acids (BAs) have been shown to exert immunomodulatory (e.g. via modulation of regulatory T cell (Tregs) function or induction of Type I IFN (IFN-I) signaling) and tissue-homeostatic functions (e.g. via direct impact on intestinal stem cells).[17–19] In particular, propionic and butyric acid, indole-3-carboxaldehyde (ICA) and deoxycholic acid have been associated with protection against GvHD in mice and humans[18]. Furthermore, specific alterations of bacteria together with metabolites, such as loss of anaerobic commensals and decrease in SCFA levels, were linked to GvHD severity.[20] In addition, there is growing evidence that metabolites mediate intra- and interspecies communication among bacteria, and influence transkingdom dynamics between bacteria, fungi and viruses[21–24].

Taken together, these studies highlight the necessity to study not only bacteria, but simultaneously also the intestinal fungal and viral communities together with metabolomics. Furthermore, the issue of how antibiotic exposure (ABX), which is frequent during allo-SCT, affects transkingdom dynamics and metabolite profiles is understudied.[6] Thus, we performed a prospective study in two transplantation centers and established a comprehensive longitudinal profiling of bacterial, fungal and viral communities together with microbiota-derived metabolites in allo-SCT patients. We identified bacterial consortia and their bacteriophages that produced immunomodulatory metabolites which were linked to improved clinical outcome. These consortia could be modulated, either inadvertently via ABX or by design via fecal microbiota transplantation (FMT), resulting in the depletion or recovery of consortia members and their associated metabolites, respectively. Via FMT we transferred these consortia to treat one patient with severe GvHD, and achieved a complete response and restoration of tissue homeostasis with reduction of $CD8^+$ cytotoxic T cells and emergence of regulatory T cells.

Results

Allo-SCT alters the composition and diversity of bacterial and viral communities and re-shapes metabolite expression profiles

From 78 patients undergoing allo-SCT enrolled in Munich (MUC; n = 25) and Regensburg (REG; n = 53), we collected stool samples to acquire a longitudinal profile of the intestinal microbiome and metabolome (Fig. 1).

By tracking the alpha diversity indices Richness and Effective Shannon beginning at Day − 7 before allo-SCT through Day + 35 after allo-SCT, we observed a loss of diversity in bacterial and viral communities,

which was lowest at Days + 14 and + 21 (Fig. 2A). Since MUC and REG centers employed different anti-fungal prophylaxis (**Supp. Table 1)**, we analyzed fungal dynamics separately for each center **(Supp.** Figure 1A). MUC patients had on average higher fungal Richness, which declined between Days − 7 and + 7 but recovered by Day + 14. However, fungal diversity by Effective Shannon remained stable across both centers (Fig. 2A).

Next, we asked whether changes in diversity correlated with intestinal abundance (density) of these communities. We observed that bacterial abundance decreased significantly after allo-SCT, and was lowest at Day + 14 (**Supp.** Figure 1B). However, unlike bacterial diversity, which remained low, bacterial abundance returned to baseline by Day + 21. Fungal abundance remained stable. Viral abundance is not shown since metagenomic shotgun sequencing is not compatible with quantification of absolute abundance.

To study the effects of allo-SCT on microbial community composition, we analyzed beta diversity and observed that bacterial communities at Day − 7 were distinct from later time-points (**Supp** Fig. 1C). Likewise, the virome of patients sampled at Day − 7 clustered together and separate from later time-points. For fungome, no time-dependent clustering pattern was observed.

To integrate the intestinal transkingdom characterization of allo-SCT patients with metabolomics, we performed a comprehensive screening of known immunomodulatory metabolite classes (SCFAs, tryptophan-derivatives and BAs). We employed targeted mass-spectrometry to analyze a total of 57 metabolites: Panel 1 consisted of SCFAs, tryptophan-derivatives and lactic acid, Panel 2 of primary and secondary, conjugated and unconjugated BAs. We found that at early time-points, especially Day − 7 and Day 0, most patients had abundant expression of Panel 1 metabolites, especially butyric, propionic and valeric acid as well as ICA (Fig. 2B), which declined at late time-points. In contrast, lactic acid was enriched at late time-points.

A large number of Panel 2 metabolites were enriched not at early but at late time-points, especially the taurine conjugates of the primary bile acid chenodeoxycholic and secondary bile acid ursodeoxycholic (UDCA) acid: taurochenodeoxycholic and tauroursodeoxycholic (TUDCA) acid (Fig. 2B **& Supp.** Figure 2A). Nonetheless, secondary BAs with known immunomodulatory functions, such as deoxycholic acid as well as lithocholic acid[25] and its derivatives (7-ketolithocholic, dehydrolithocholic, glycolithocholic acid) displayed early enrichment, and similar to Panel 1 metabolites, were abrogated at late time-points.

By performing principal component analysis (PCA), we observed that expression profiles of Panel 1, but not Panel 2 metabolites, at Day − 7 were distinct from late time-points (**Supp.** Figure 2B).

Interestingly, certain metabolites such as ICA[18], acetic acid[26] as well as deoxycholic acid[27] were increased only at early time-points. These metabolites are potent activators of IFN-I signaling, which is assumed to positively or negatively modulate GvHD depending on the timing of IFN-I activation.[26,28] Henceforth we will refer to them as “IFN-I-inducing metabolites (IIMs)”.

Taken together, we observed that distinct bacterial and viral communities at Day − 7 were reshaped during the course of allo-SCT, which matched the timing of alterations of the expression profile of microbiota-derived metabolites. Specifically, bacterial diversity and abundance and viral diversity reached its nadir at Day + 14, which was accompanied by a drastic reduction of SCFAs and IIMs.

Multi-omics factor analysis reveals a microbiome signature of metabolite-producing bacteria and their bacteriophages

We employed multi-omics factor analysis (MOFA) to identify patterns of covariation across all three intestinal communities and microbiota-derived metabolites with the goal of identifying microbiome signatures associated with production of SCFAs and IIMs. We opted for an unbiased approach, and decided against inputting clinical and sample meta-data such as diagnosis or time-point for model generation, in order to identify which factors inferred only by multi-omics explained metabolite production.

Viral and bacterial composition, but not fungal, contributed most to total variance across all patient samples (Fig. 3A). Variance explained by the bacteriome was concentrated in Factors 1 and 3 (Fig. 3B). Variance explained by the virome was divided between Factors 1 through 5. Next, we explored whether these transkingdom factors co-varied with metabolites. Panel 1 metabolites were positively correlated with Factors 1, 3 and 10 and negatively correlated with Factor 2, with the exception of lactic acid, which followed an opposing trend (Fig. 3C, **left panel**). Factor 1 was also positively associated with the Panel 2 metabolites deoxycholic and dehydrolithocholic acid, but negatively correlated with TUDCA and UDCA (Fig. 3C, **right panel**). Since Factors 1 and 3 explained a large proportion of the total variance, captured co-variations across bacterial and viral kingdoms, and correlated with intestinal concentration of SCFAs and IIMs, we decided to focus on these for downstream analysis. For each Factor, we characterized the top weights by kingdom, i.e., the bacterial, fungal and viral taxa most positively or negatively associated with that Factor. Our goal was to determine which specific taxa contributed most to the metabolite-associated Factors 1 and 3, to learn which taxa were important for metabolite production.

Factor 1 was linked to the obligatory anaerobic bacterial families *Lachnospiraceae*, *Oscillospiraceae* and *Eubacteriaceae* (Fig. 3D, **top panel**). We detected the genera *Ruminococcus*, *Subdoligranulum* and *Blautia*, which at species-level have been shown to produce butyrate.[29,30] Only *Enterococcus* was strongly negatively correlated with Factor 1. The fungal genera *Helotiales* and *Aureobasidium* were positively correlated with Factor 1, while members of the *Aspergillaceae* family were negatively correlated with this Factor (**Supp.** Figure 3A, **left panel**). All viral taxa that were identified by Factor 1 were prokaryotic viruses or bacteriophages, and nine out of ten were negatively correlated with this Factor. These bacteriophages were predicted to infect *E. coli*, *Enterococcus*, *Hungatella* and *Staphylococcus aureus* (**Supp.** Figure 3A, **right panel**). Factor 3 was linked to the genera *Flavonifractor*, *Blautia* and *Sellimonas*, from the bacterial families *Lachnospiraceae, Oscillospiraceae and Clostridiaceae* **(**Fig. 3D, **bottom panel)**. For fungome, only *Pichia* was strongly correlated with Factor 3 (**Supp.** Figure 3A, **left panel**). As in Factor 1, all top ten viral weights identified by Factor 3 were bacteriophages predicted to infect *Flavonifractor*, *Hungatella*, *E. coli*,

Clostridioides and *Anerotruncus colihominis* (**Supp.** Figure 3A, **right panel**). Taken together, Factors 1 and 3 defined a microbiome signature linking SCFA and IIM expression with bacteria from the *Lachnospiraceae* and *Oscillospiraceae* families which co-varied with their associated bacteriophages, i.e., *Flavonifractor* and *Flavonifractor*-type bacteriophage. Strikingly, this microbiome signature was characterized by suppression of *Enterococcus* and *Enterococcus*-type bacteriophages.

To identify which intestinal bacteria contributed most to metabolite production, we tested the correlation of each bacterial genus against different metabolites. Across all samples, *Lachnospiraceae* were significantly correlated with butyric acid ($p \leq 0.0001$) and *Bacteroides*[31] with propionic acid ($p \leq 0.0001$) (Fig. 3E, **Supp.** Figure 3B). In contrast, *Enterococcus* was negatively correlated with SCFAs, but positively correlated with lactic acid (**Supp.** Figure 3B).

Since some bacteriophages identified by Factors 1 and 3 were assigned to *E. coli* via host prediction, but *E. coli* was not a top bacterial weight in either Factor, we wondered if these bacteriophages targeted other bacteria. Therefore, we performed a correlation analysis of bacterial and viral abundance at genus level and observed that several bacteriophages were highly correlated with the *Lachnospiraceae* family members *Blautia* and *Sellimonas* (Fig. 3F, **Supp.** Figure 3C), suggesting a previously unknown association between bacteriome and virome which remains to be explored.

In summary, we identified a SCFA and IIM-producing consortia comprised of bacteria from the *Oscillospiraceae* and *Lachnospiraceae* families and their associated bacteriophages that were negatively correlated with *Enterococcus* and *Enterococcus*-associated bacteriophages.

Allo-SCT disrupts a specific metabolite-producing bacterial consortia and their bacteriophages

Next, we asked how allo-SCT altered intestinal community composition and how this affected production of metabolites. At early time-points, we detected an enrichment of *Lachnoclostridium*, *Lachnospiraceae* family members and *Flavonifractor* (Fig. 4A, **top panel**). These changes corresponded to an early enrichment of *Lachnospiraceae* and *Oscillospiraceae* at family level (**Supp.** Figure 4A). The taxonomic composition at late time-points was very different: at genus level, *Enterococcus*, *Lactobacillus* and *Streptococcus* were highly enriched.

We performed the same taxonomic analysis for the intestinal fungome. In line with stable alpha and beta diversity scores, we did not observe any time-dependent patterns, with the exception of an early enrichment of *Aspergillaceae* at family level (**Supp.** Figure 4B).

Viral binning at genus level remains challenging due to a limited number of reference sequences stored in public databases, therefore we decided to analyze viral community composition at order and family level. Although previous studies[15] have characterized eukaryotic and prokaryotic viruses separately, we began by querying the entire intestinal virome. We noted that prokaryotic were in much higher abundance than eukaryotic viruses. We detected *Siphoviridae*, *Podoviridae* and *Myoviridae* (Fig. 4A, **bottom panel**), of the

order *Caudovirales* (**Supp.** Figure 5A**)**. We then analyzed the dynamics of the two most common eukaryotic reads: vertebrate and plant viruses. Although we detected prokaryotic reads in all patient samples (100%), reads assigned to vertebrate and plant viruses were only detected in 50% and 70% of samples, respectively (**Supp.** Figure 5B). We also investigated the dynamics of vertebrate viruses known to target human hosts: With the exception of *Poxviridae*, which was detected in approx. 40% of patients at Day − 7 and decreased by more than 50% by Day + 7, vertebrate viral reads were rare among our cohort (**Supp.** Figure 5C).

Next, we characterized the expression of metabolites associated with Factors 1 and 3 before and after allo-SCT. We observed that levels of SCFAs and IIMs declined significantly at Day + 7 and reached a minimum at Day 21 (Fig. 4B). Butyric acid (-90%), valeric acid (-95%), lithocholic acid (-99%) as well as dehydrolithocholic acid (-98%) were altogether depleted at this time-point. In contrast, the secondary BAs TUDCA (20-fold) and UDCA (3-fold) were significantly increased. Thus, a microbiome signature consistent with the previously identified SCFA and IIM-producing bacterial consortia was only detectable at early time-points. After allo-SCT these consortia were disrupted, resulting in a significant decrease of metabolite levels.

High-level expression of SCFA and IIM are associated with better outcomes after allo-SCT

Previous studies have shown that bacterial alpha diversity at the time of neutrophil engraftment, stratified into high and low diversity groups, was predictive of outcome in allo-SCT[8]. We confirmed that patients with high bacterial diversity had higher overall survival (OS), reduced incidence of GI-GvHD and less transplant-related mortality (TRM) (**Supp.** Figure 6), also when considering multivariable adjustment (**Supp. Table 2)**. In contrast, neither fungal nor viral diversity was significantly correlated with OS (**Supp.** Figure 6).

Since we showed that the reduction of bacterial and viral diversity was accompanied by disruption of metabolite-producing bacterial consortia, and that low alpha diversity was associated with worse outcome, we predicted that low levels of SCFAs and IIMs would be deleterious in allo-SCT patients. Indeed, expression of SCFAs and IIMs between Days 7 to 21 correlated positively with OS (Fig. 4C) and negatively with TRM (**Supp. Figure 7**). Due to their association with improved clinical outcome, these metabolites are henceforth referred to as “protective metabolites”.

GI-GvHD is characterized by Enterococcus domination and displacement of protective bacterial consortia and their bacteriophages

Next, we asked whether GI-GvHD altered bacterial, fungal and viral communities, impacted the identified bacterial consortia and thereby depleted protective metabolites. Therefore, we stratified allo-SCT patients into two groups: those with clinical diagnosis of GI-GvHD of any severity and those without. In line with previous studies, we observed significantly lower bacterial Richness in GI-GvHD patients compared to control allo-SCT patients (Fig. 5A). Viral followed bacterial dynamics, and we detected significantly lower

viral Richness in patients with GI-GvHD. We did not observe any difference in fungal alpha diversity between the two groups (**Supp. Figure 8A**). Although we did not observe statistically significant differences in bacterial or viral diversity measured by Effective Shannon, nor in bacterial abundance (**Supp. Figure 8B**), there was a trend towards reduced scores in GI-GvHD patients. Beta diversity analysis showed major differences in bacterial and viral, but not fungal community compositions in patients with or without GI-GvHD (**Supp. Figure 8C**).

On average, samples from GI-GvHD patients had a bacterial diversity of less than 10 by Effective Shannon (Fig. 5A), suggesting that the bacterial community was made up of only a few or single taxa. Therefore, we measured intestinal domination, defined as a single taxon being more than 50% abundant in a patient sample (Fig. 5B). Control allo-SCT patients retained a much more heterogenous group of taxa, while in GI-GvHD patients specific taxa contributed to a GvHD-related microbial signature: *Enterococcus*, *Lactobacillus*, *Streptococcus and Staphylococcus*. Fungome analysis revealed that domination by *Naumovozyma* occurred earlier and at higher rates in GI-GvHD patients than in control allo-SCT patients. On average, control patients retained a heterogenous group of taxa, while domination by *Candida* and *Debaryomyces* were over-represented in GvHD patients (**Supp. Figure 8D**). The bacteriophage family *Myoviridae* was more abundant in control allo-SCT, while *Podoviridae* and *Siphoviridiae* were more abundant in GI-GvHD patients (**Supp. Figure 8E**).

GI-GvHD patients presented with lower levels of protective metabolites (Fig. 5C): With the exception of lactic acid (increased), expression of acetic, butyric, propionic and valeric acid declined significantly. Of Panel 2, only lithocholic acid was significantly different and depleted in GI-GvHD, while TUDCA and UDCA levels were comparable between both groups (**Supp. Figure 8F**).

Taken together, our data suggests that despite a reduction of bacterial and viral diversity in control allo-SCT patients, these patients retained a more homogenous community composition and were able to maintain low-level production of protective metabolites after allo-SCT. In GI-GvHD patients, domination by *Enterococcus* displaced the identified bacterial/bacteriophage consortia and protective metabolites were depleted.

Antibiotics impact bacterial consortia and their bacteriophages and alter metabolite expression profiles

Almost always during allo-SCT broad-spectrum antibiotics (ABX) are administered, due to febrile neutropenia and infections. In our study, 100% of MUC and 94% of REG patients received ABX during their hospital stay (**Supp. Table 3**) as per center-specific standards (**Supp. Table 1**). However, exposure to ABX is a major confounder in microbiome research. Indeed, we observed bacterial shifts that are consistent with ABX exposure (abolishment of families from the *Clostridia* and *Erysipelotrichia* classes, domination by *Enterococcus*)[32]. Therefore, we performed beta-diversity analysis to test whether ABX altered intestinal community composition and suppressed the identified bacterial/bacteriophage consortia. Indeed, ABX resulted in major and significant changes to bacterial and viral, but not fungal, community compositions (**Supp. Figure 9A**). ABX also resulted in a significant decrease of bacterial and viral, but not fungal,

Richness and Effective Shannon scores (Fig. 5D) as well as reduced bacterial but not fungal abundance (**Supp. Figure 9B**). In particular, exposure to ABX resulted in a decrease of *Lachnospiraceae* and *Oscillospiraceae* family members, but increase of *Enterococcus* (Fig. 5E). Fungal communities were less impacted by antibiotics, but responded with an increase of *Aspergillus* (**Supp. Figure 9C**). *Siphoviridae* and *Myoviridae* bacteriophage families were increased after exposure to ABX (**Supp. Figure 9D**).

ABX significantly altered expression profiles of Panel 1 and Panel 2 metabolites (**Supp. Figure 9E**). Specifically, ABX significantly impaired production of protective metabolites, and completely abolished expression of butyric acid, valeric acid, ICA and lithocholic acid. In contrast, lactic acid was increased in ABX-treated patients (Fig. 5F). Taken together, the effect of ABX was consistent with suppression of the identified bacterial consortia resulting in near-total depletion of protective metabolites.

We observed that loss of bacterial and viral diversity and depletion of protective metabolites impaired outcome after allo-SCT and were associated with GI-GvHD and ABX. Conversely, we hypothesized that allo-SCT patients that maintained a diverse microbiota composition and sustained production of protective metabolites would be protected. Therefore, we designed an algorithm to identify patients with the highest and lowest average alpha diversity and analyzed their clinical course together with multi-omics (**Supp. Figure 10, Supp. Table 4**). An adverse clinical course characterized by early exposure to ABX and development GI-GvHD was associated with the taxonomic and metabolomic changes described above, while a favorable clinical course underscored our observation that upkeep of even low-level production of metabolites protected from transplant-related complications.

Fecal microbiota transplant resolves GI-GvHD and restores tissue homeostasis via metabolite-producing consortia

Based on our data, we hypothesized that GvHD-related microbial signatures could in principle be restored via FMT. We performed FMT to treat a case of severe steroid- and ruxolitinib refractory GI-GvHD. The patient, a 59-year-old female, suffered from high-risk myelodysplastic syndrome and underwent allo-SCT from an HLA-C-mismatch unrelated donor (**Supp. Table 4**). At Day + 60 she first developed grade I GI-GvHD. At Day + 290, she was admitted to the hospital with severe grade IV GI-GvHD (clinical grading), which was unresponsive to steroids and immunosuppressants (Fig. 6A). We obtained colon tissue biopsies, and detected crypt apoptosis, exploding crypt cells and loss of crypts in the large intestinal epithelium, consistent with acute GvHD grade 3 (histopathological grading)[33,34] (**Supp. Figure 11A**).

On Day 0 (Day + 306 after allo-SCT) the patient received the first of two FMTs from a healthy, unrelated donor via colonoscopy. We performed a second FMT on Day + 8. Both FMTs were from the same donor, who previously underwent donor screening (comprehensive panel of enteric pathogens, see **Supp. Table 5**).

At Day − 1, we observed low bacterial, fungal and viral alpha diversity (Fig. 6B, **top**) and domination by *Enterococcus* and *Nakaseomyces* (Fig. 6C). At Day + 7, bacterial diversity remained low, likely due to FMT-engraftment failure because of concomitant administration of antibiotics during *Campylobacter*

septicemia. After the second FMT at Day + 8 we observed a rapid recovery and complete response (CR) of GI-GvHD, evident by reduction of diarrhea frequency, lessening of abdominal pain and improvement of performance status (ECOG from 3 to 1), which allowed the tapering of steroids as well as immunosuppression. At Day + 12, the patient's microbiota showed signs of recovery and approximation towards the donor's community composition, with detection of *Blautia*, *Lachnoclostridium*, *Lachnospiraceae*, *Subdoligranulum* and *Ruminococcus* (Fig. 6C) (within the *Lachnospiraceae* and *Oscillospiraceae* families*)*. FMT restored expression of *Myoviridae* and reduced *Siphoviridae* bacteriophages. Next, we measured levels of Panel 1 and 2 metabolites in the donor and recipient. There was no detectable production of SCFAs and IIMs in the recipient at Day − 1 (Fig. 6B, **bottom** & **Supp. Figure 11B**). After FMT, at Day + 12, resolution of GI-GvHD in the recipient was accompanied by abundant expression of protective metabolites, mirroring the rich and diverse metabolite expression profile observed in the donor.

At nine months follow-up, the patient remained in CR from GI-GvHD, at which time we obtained another biopsy (Day + 289) and observed a significant improvement of the large intestinal epithelium: Only single apoptotic cells were detectable within the otherwise regularly structured mucosa. The crypts appeared regenerated and infiltrating lymphocytes were sparse (**Supp. Figure 11A**).

To obtain first insights into the mechanisms underlying microbiome-based treatment of GvHD as basis for future studies, we analyzed immune populations in the colon by ChipCytometry before and after FMT (Fig. 6D). Before FMT, the large intestinal epithelium was densely infiltrated by $CD8^+$ cytotoxic T cells and the CD4:CD8 effector T cell ratio was heavily skewed towards $CD8^+$, consistent with allogeneic T cell responses in GvHD (Fig. 6E, **top**). After FMT, the CD4:CD8 ratio was normalized, and we detected a higher number of Tregs (Fig. 6E, **bottom**), which can mitigate allogeneic immune responses, promote tissue healing[35] and are known to be activated by microbiota-derived metabolites including SCFAs[36]. Although this requires confirmation in larger cohorts, the detection of *Lachnospiraceae* and *Oscillospiraceae*, as well as of protective metabolites in this patient, may suggest that FMT can transmit protective, metabolite-producing bacterial consortia which stably engraft resulting in restoration of tissue homeostasis and thus amelioration of symptoms in severe GI GvHD.

Discussion

To our knowledge, this is the first two-center study to integrate time-dependent taxonomic shifts in bacteriome, fungome and virome with targeted mass-spectrometry of immunomodulatory microbiota-derived metabolite in a longitudinal fashion in allo-SCT patients. We identified bacterial/bacteriophage consortia linked to the production of SCFAs and IIMs which were associated with better outcome after allo-SCT. We found that allo-SCT drastically reduced bacterial and viral diversity as well as bacterial abundance, thereby disrupting the identified metabolite-producing bacterial consortia comprised of *Lachnospiraceae* and *Oscillospiraceae* families and instead promoting domination by *Enterococcus* (graphical summary **Supp. Figure 12**). These time-dependent taxonomic alterations align with previous

studies which have classified bacteria as protective or deleterious according to their association with GvHD, *Enterococcus* being characteristic of GvHD-related microbial signatures.[2,8,37,38]

In contrast, fungal diversity and abundance remained stable during allo-SCT and did not decline in GI-GvHD patients[13,39]. One recent study observed an increase in culturable fungi after allo-SCT concomitant with reduction of intestinal bacterial abundance.[40] Another culture-based study identified a subset of patients in which *Candida parapsilosis* complex species correlated with worse OS and higher TRM.[13] While we detected *Candida*, we did not observe time-dependent changes in its abundance via ITS amplicon sequencing. We did however observe the domination of *Candida* genus in GI-GvHD patients, the most common cause of fungal infections in immunocompromised patients.

Using MOFA we identified consortia of bacterial families – *Oscillospiraceae* and *Lachnospiraceae* – and bacteriophages associated with the increase of SCFAs and IIMs. These taxa were among those most highly depleted after allo-SCT. We identified the bacteriophages associated with changes in metabolite-producing bacterial taxa such as *Blautia* and *Sellimonas* but also in deleterious taxa such as *Enterococcus*. In patients, these protective bacterial/bacteriophage consortia were linked to lower *Enterococcus* and lactic acid abundance, a metabolite which was recently associated with T cell exhaustion and relapse of leukemia after allo-SCT[41]. We uncovered a previously unknown association between bacteriome, virome and metabolite-production, which calls attention to current concepts in design of LBPs[42] employing only bacteria, and may suggest an important role for bacteriophages in synthetic consortia engineered to produce metabolites. Whether bacteriophages are necessary or contributory for the production of IIM and SCFA by consortia members merits further preclinical studies.

We observed that changes in intestinal bacterial diversity, abundance and community composition were accompanied by reduced bacteriophage richness and abundance over time and especially in GI-GvHD patients. Our results partially align with Legoff et al.[43], which characterized the longitudinal gut virome in 44 patients after allo-SCT and showed an increase of eukaryotic viral contigs predicted to infect vertebrate hosts after allo-SCT, and in GvHD patients an increase of vertebrate persistent DNA viruses as well as decrease of bacteriophage richness. We did not detect major alterations in the intestinal eukaryotic virome. Instead, we observed a high abundance of prokaryotic viruses from *Caudovirales* order. Considering that bacteria make up more than 50% of total solids in human feces[44], and that allo-SCT drastically altered bacterial communities, we interpreted these findings to suggest that viral alterations in allo-SCT occur at the level of bacteriophages that shift in response to factors affecting their host bacteria. This is consistent with a recent MOFA in patients with sepsis at the intensive care unit, showing that bacteria and their corresponding bacteriophages co-varied in Factors driven by antibiotic perturbation[45]. Nonetheless, although we methodically analyzed eukaryotic contigs, our viral sequencing pipeline is optimized for dsDNA bacteriophage detection and does not allow eukaryotic RNA-virus detection.

Microbiota-derived metabolites have been shown to protect from GvHD in animal models.[17,18,25,46] By screening for specific immunomodulatory metabolites in unprocessed feces via targeted mass-spectrometry we deliberately chose a hypothesis-driven over discovery-driven approach to maximize reliability and reproducibility. We favored the hypothesis that identification of intestinal metabolites affecting local tissue homeostasis and mucosal immunoregulation could be used for engineering LBPs for microbiome-based therapies. Besides the well-characterized SCFAs, we observed that allo-SCT reshaped expression patterns of intestinal metabolites which were not previously described in the human allo-SCT setting, such as valeric acid, ICA, certain BAs and lactic acid.

In 2019 Michonneau et al. performed a multicentric screening of metabolites in serum samples of allo-SCT recipients and donors via untargeted mass spectrometry. At the onset of GvHD, they observed a decrease in tryptophan metabolites including 3-indoxyl sulfate, indolacetate (IAA) and other aryl hydrocarbon receptor (AhR) ligands.[47] Although our Panel 1 included IAA, we detected this compound in fewer than 10% of intestinal samples. Instead, we observed that the tryptophan-derivate ICA, which was recently shown to target AhR and protect mice from metabolic syndrome[48] as well as GvHD[18], was significantly reduced after allo-SCT and in GI-GvHD patients. In the same study, serum secondary BAs UDCA and TUDCA were increased in patients with acute GvHD. We observed an increase of intestinal UDCA and TUDCA at late time-points after allo-SCT, although levels were not significantly different between GI-GvHD patients compared to controls. Together, this suggests a specific, negative effect of allo-SCT and GvHD on Panel 1 metabolite expression.

Consistent with numerous studies we observed that higher bacterial diversity was associated with better OS, less GI-GvHD and less TRM.[2,8,39,49] Although reduction of viral diversity was associated with GI-GvHD, it was not predictive of outcome after allo-SCT. Yet, we linked expression of SCFAs and IIMs to clinical outcome after allo-SCT, and showed that patients with higher-level metabolite expression in the post-transplant period had improved OS, providing a rationale for development of microbiota-derived metabolites as biomarkers.

In GI-GvHD patients, deleterious taxa[20] dominated more quickly and were more likely to achieve absolute domination. *Enterococcus*, the most frequently dominant taxa, was significantly correlated with lactic acid, and – since lactic acid is a major fermentation product of intestinal lactose – may corroborate in humans the recent work by Stein-Thoeringer et al.[38], showing that lactose drives expansion of *Enterococcus* and promotes GvHD. Intestinal levels of lactic acid may thus be useful as biomarker for absence of protective bacterial/bacteriophage consortia.

Antibiotics significantly impact intestinal bacteria.[2,50] In 2020, Payen et al. described that loss of anaerobic commensals and subsequent decrease of intestinal SCFA levels, specifically acetate, propionate and butyrate, were associated with severe aGvHD.[20] However, since all patients were on antibiotics at the time of sampling and during follow-up, they were unable to address the impact of antibiotics on microbiota or metabolites. Romick et al. observed a negative correlation between intestinal

butyrate and propionate and exposure to antibiotics[51]. To the best of our knowledge this is the first study in patients that has characterized the impact of antibiotics on intestinal transkingdom diversity and community composition as well as their metabolites. Intriguingly, while antibiotics had minimal effects on fungal communities, they significantly altered the intestinal bacteriome and virome. In line with our previous work[52], we observed that antibiotics depleted protective metabolites. In ABX-treated and GI-GvHD patients alike, metabolite levels declined, and some metabolites such as valeric acid, ICA and lithocholic acid were altogether abolished. We have previously shown that timing of antibiotic therapy impacts the intestinal bacteriome[53], and it stands to reason that liming ABX exposure or altering timing of ABX could be used to modulate metabolite levels and with it, clinical outcome.

Fecal microbiota transplantation (FMT) is a microbiome-based therapy against GI-GvHD, which has achieved partial and complete responses in allo-SCT patients suffering from steroid-refractory GI-GvHD in early clinical trials[54–56] and has recently entered Phase 3 clinical testing[57]. So far, FMT has been associated with improved GI symptoms, restoration of diversity of the intestinal bacterial community and partial engraftment of donor taxa[58,59]. However, response rates and durability of responses remain suboptimal. A recent study performed a longitudinal, transkingdom characterization in a single GvHD patient treated with FMT[60]. After multiple FMTs, bacterial diversity gradually recovered. The fungome responded with increase of abundance in several species while the overall diversity decreased. As for virome, they characterized the top 50 eukaryotic viruses but found them to be present only at low abundances and largely unchanged after FMT. In contrast, they observed an increase in bacteriophage abundance and diversity after FMT, with *Caudovirales* replacing the patient's initial *Microviridae* lineage. Expanding upon this study[60], we incorporated metabolomic read-outs, and present how *Enterococcus* domination and loss of metabolite production could be overcome by transferring the donor's metabolite-producing bacterial consortia and their bacteriophages, which resulted in high-level production of these metabolites in the recipient. As an exploratory approach, we characterized microbiome-related changes to the intestinal epithelium and mucosal immune subsets, and observed restoration of the intestinal barrier, improvement of the CD4:CD8 effector T cell ratio, and re-emergence of Tregs. However, this represents a single case and requires confirmation in larger cohorts. Furthermore, since the second biopsy was obtained at a later time-point, we are cautious to conclude that improvements resulted directly from FMT. Nevertheless, our observation that Tregs were increased after FMT are supported by a recent study which linked microbial diversity to $CD4^+$ T cell count in allo-SCT patients[61].

Building on our findings we suggest the following strategies for designing microbiome-based therapies: (1) optimization of antibiotic therapy (e.g. via timing of ABX exposure) if clinically feasible to limit collateral damage to metabolite-producing consortia, (2) standardization of FMT based on defined bacterial and bacteriophage consortia such as the one consisting of *Oscillospiraceae* and *Lachnospiraceae* identified herein, (3) administration of LBPs comprised of synthetic consortia engineered to produce SCFAs and IIMs and/or metabolite combination drugs containing defined SCFAs and IIMs. Our research provides a strong rationale for therapeutic use of these immunomodulatory

metabolites via modulation of intestinal bacterial and viral communities as new frontier in microbiome-based therapies aimed at improving clinical outcomes after allo-SCT.

Methods

Study design

We employed a multi-centric study of patients undergoing allogeneic stem-cell transplantation to assemble an integrated, longitudinal understanding of the transkingdom taxonomic and metabolomic shifts in each individual. We prospectively collected stool samples at calendar-driven and event-driven timepoints for characterization of the intestinal bacterial, fungal and viral community composition. The bacteriome and fungome were characterized via 16S and ITS amplicon sequencing, while for virome, we first purified viral particles via combination of filtration and ultracentrifugation steps, followed by deep viral whole genome shotgun sequencing.[62] In parallel, each sample was assayed by mass-spectrometry for expression of microbiota-derived metabolites including short chain fatty acids, indole derivatives or bile acids (>44 different BAs including primary, secondary and conjugated BAs). Upon this extensive data set we employed multi-omics factor analysis (MOFA). Bio samples were referenced with extensive clinical metadata, including GvHD, anti-infective medication and laboratory findings.

Patient stool samples were collected at pre-defined calendar- and event-driven time-points in accordance with IRB-approved study protocols (see “Patient characteristics” below). Measurements were taken from distinct stool samples of individual patients. The stool samples comprised a unique bio-sample collection and have been completely used for the analyses performed in this study. No additional material is available. The data sets generated and analyzed during the current study are available in the European Nucleotide Archive (https://www.ebi.ac.uk/ena/browser/home).

Patient characteristics

Stool samples were collected at the University Hospital of the Technical University of Munich and the University Hospital Regensburg. At both centers, 78 patients undergoing allogeneic stem-cell transplantation were enrolled (Munich: n= 25 between 2019-2021, Regensburg: n=53 between 2018-2021) in a prospective, observational study after informed consent and in accordance with IRB-approved study protocols (Munich: “Ethikkommission der TU München” IRB 295/18 S; Regensburg: “Ethikkommission bei der Universität Regensburg” IRB 02/220, 14-101-0047, 17-619-101). Sampling occurred at pre-determined time-points (calendar-driven) or in response to clinical occurrences (event-driven) **(Figure 1A)**. Sampling was carefully coordinated between both centers and performed weekly during the peri-transplant period. Samples were obtained on or one to two days around the specified time-points and stored at -80 °C within 4 hours until further processing. Calendar-driven time-points were:

- at in-patient admission to the bone marrow transplantation unit for initiation of conditioning therapy (Day -7)
- at the day of the allogeneic stem-cell transplantation (Day 0)
- at one week after allo-SCT (Day +7)
- at two weeks after allo-SCT (Day +14)
- and weekly thereafter until patients were discharged or up until Day +35 after allo-SCT, whichever occurred first

Event-driven time-points were the occurrence of acute gastrointestinal GvHD, weekly during occurrence of GI-GvHD and after resolution of acute GI-GvHD.

Patient characteristics including age, gender, diagnosis and survival were similarly distributed amongst both cohorts (**Figure 1B**).

Graft-versus-Host Disease

Gastrointestinal GvHD occurred in approximately 50% of patients. A third of these patients developed severe GI-GvHD, defined as GI-GvHD grade 2 to 4. At occurrence of GvHD, patients received i.v. corticosteroid therapy, the standard-of-care first line treatment at both centers. Steroid resistance was defined according to MAGIC criteria.[63] Stool samples of patient with active GI-GvHD were labeled as such, and compared to time-point matched samples from patients without GvHD (control allo-SCT patients).

Antibiotics

Patient samples were grouped according to antibiotic status: Samples categorized as “no ABX” had no exposure, but once a patient was started on antibiotics the first and all subsequent samples were classified as “ABX”. In addition, all samples were annotated according to concomitant anti-infective prophylaxis (site-specific standards, see **Supp. Table 3**), as well as antifungal and antiviral therapy (**Supp. Table 2**) at the time of sampling.

Survival Analysis

After follow-up of one year, 68 patients were alive (**Figure 1**). Two patients died from relapse, 13 died from transplantation related complications (mainly GvHD and infections). Overall survival (OS) and cumulative incidences of transplant-related mortality (TRM) and GvHD were estimated and presented as hazard ratios with 95% confidence interval. Patients were stratified into higher-diversity and lower-diversity groups according to the center-specific median diversity value (inverse Simpson index for bacteriome, fungome and virome, respectively) observed in the samples obtained at days +7 until +21. When a patient had more than one sample, the mean value was used for analysis. In the same way patients were

stratified into higher and lower metabolite levels according to the center-specific median intestinal metabolite level observed between days +7 and +21. IBM SPSS 25 was used for analysis.

Individual case reports

For clinical cases of individual patients (**Supp. Figure 10**), we identified the top and bottom patients with the highest and lowest mean alpha diversity for both MUC and REG centers. Patients with a baseline (Day -7) sample and minimum of 3 additional longitudinal samples were stratified into high or low bacterial diversity by mean Effective Shannon score across all time-points. We characterized Patients 1 and 2, with highest and lowest alpha diversity, respectively. Patient samples were aligned with clinical metadata including body temperature, white blood count (WBC), C-reactive protein (CRP), administration and timing of anti-infective medication including antibiotics as well as of immunosuppressive therapy. Age, underlying disease, donor status, conditioning regimen, incidence of GI-GvHD and additional clinical information is provided in **Supp. Table 4**.

Bacteriome Analysis

Extraction and quantification of bacterial and fungal nucleic acids

For microbiome analysis stool samples were collected in magiX PB1 microbiome preservation buffer (microBIOMix GmbH, Regensburg) and transferred to the laboratory within four hours (MUC) or within one day (REG). Immediately after receipt, stool suspensions were frozen and stored at –80 °C until further processing. To extract fungal and bacterial nucleic acids, stool suspensions were thawed and ~ 50 mg stool were mixed with a pool of three spike bacteria *Alcanivorax borkumensis*, *Agrobacterium radiobacter*, and *Alicyclobacillus acidiphilus* to 2e+7, 1.6e+7 and 6e+8 16S rDNA copies per sample, respectively. These species served as internal process controls.[64] Cells were lysed by applying a repeated bead-beating protocol using 0.5 mm yttria-stabilized zirconium oxide beads (MP Biomedicals, Eschwege, Germany) on a TissueLyser II instrument (Qiagen) followed by Proteinase K digestion (Roche, Mannheim, Germany) and freezing and thawing. DNA was purified by means of the MagNA Pure 96 instrument (Roche) using the MagNA Pure 96 DNA and Viral NA Large Volume Kit (Roche).

Amplification and semiconductor-based sequencing of V1-3 16S rDNA and fungal Internal Transcribed Spacer 1 Regions (ITS1) regions

V1 to V3 hypervariable regions of bacterial 16S rRNA genes were amplified from a total of 1e+7 bacterial 16S rDNA copies for each sample using the forward primer S-D-Bact-0008-c-S-20 containing sample-specific barcode and sequencing adaptor sequences together with reverse primer S-D-Bact-0517-a-A-18 containing a 3’-P1 adapter sequence. Fungal Internal transcribed spacer regions 1 (ITS1) were amplified

from 5 ng DNA using primer pairs ITS1-30F/ITS1-217R[65] containing barcode and sequencing adaptors. The resulting amplicons were purified with MagSi-NGSPREP Plus beads (Steinbrenner Laborsysteme, Wiesenbach, Germany). Amplicon copy numbers were determined using the KAPA Library Quantification IonTorrent Kit (Roche). DNA library was prepared by pooling equimolar concentrations of adaptor-labeled amplicons. Re-amplification of the final sequencing library by isothermal amplification, chip loading and high-throughput sequencing which was carried out using the IonChef™ instrument and the IonTorrent™ Genestudio S5 Plus sequencer (Thermo Fisher Scientific, Waltham, USA).

Bacteriome and Fungome Quantification

To allow for comparisons across different kingdoms we performed absolute quantification of bacteria and fungi. Bacterial and fungal DNA was quantified by real-time PCR using pan-bacterial (16S) and pan-fungal (28S) specific primers, respectively, and amplicon copy numbers were normalized to gram of stool. Quantification of 16S rDNA copies by qPCR was carried out as described earlier.[66] Fungal load was quantified by using primers NL1 and 260R and a 28S rDNA-specific FAM-labelled hydrolysis probe.[67] DNA fragments of *Penicillium roqueforti* 28S rDNA amplified with NL-1/NL-4 primers which were cloned into the pJET1.2 vector (Thermo Fisher Scientific) were used as quantification standard.

Bacteriome and Fungome Data Analysis

Raw sequencing reads were subjected to Trimmomatic[68] (0.39) for sliding window trimming applying a windows size of 25 and a quality cutoff of 20. Cutadapt[69] (3.4) was used for demultiplexing and removal of sequencing adapters and 16S-specific PCR primer sequences. Amplicon sequence variants (ASV) were generated in R (4.1.0) from demultiplexed reads using a dada2 (1.22)-based workflow[70]. Standard parameters were used, except gap penalty, band size and OMEGA_A values, which were set to –1, 32 and 1e-30 respectively. Taxonomy of ASVs was predicted by the IDTAXA algorithm of the DECIPHER[71] package after matching to the SILVA[72] 138.1 release 16S reference database (bacteria). The February 2020 release of the Unite database[73] (fungal ITS) was used to predict fungal taxonomy. Alpha- and beta-diversity analyses were conducted applying the phyloseq[74] package version 1.36. Species Richness was represented by summarized ASV. Effective Shannon index was calculated by the exponent of the Shannon entropy[75]. Means of groups were compared with the Wilcoxon Rank Sum test (two-sided) adjusted for multiple comparisons with the Bonferroni method. Beta diversity was calculated by weighted Unifrac and distances between time-points or groups (No ABX versus ABX; No GI-GvHD versus GI-GvHD) were projected in a principal coordinate analysis (PCoA). Principal coordinates were calculated from weighted UniFrac distances after cumulative sum scaling of ASV counts. Significance of group differences were analyzed by PERMANOVA using the pairwiseAdonis[76] (0.4) package. For Pearson correlation analyses, the correlation coefficient and p-value were calculated with the ggpubr package. Linear discriminant analysis based on the LEfSe and generation of cladograms were carried out with the microbiomeMarker package[77] (1.0.1) after total sum scaling and applying alpha level and log2 fold

change cutoffs of 0.01 and 2 respectively. Heatmaps for most abundant fungal and bacterial taxa were generated from summarized ASV reads after centered log-ratio normalization. Dominant taxa were identified by summarizing bacterial and fungal reads with a maximum relative genus-level abundance above 50 percent and plotted by ggplot2 (3.3.5). Plots for alpha diversity and bacterial and fungal loads were generated by ggpubr (0.4). P-values are shown either as exact value (Figure Legends) or as P-value summary (Figures): ns…not significant (p > 0.05); *…p <0.05; **…p <0.01; ***…p <0.001; ****…p <0.0001.

Virome Analysis

Virome sequence processing

Low-quality bases and adaptors of raw sequences were removed using fastp (v0.20.1)[78]. The remaining reads were deduplicated by dedupe.sh from bbmap suite (v38.76)[79], and clean reads were assembled into contigs by metaSPAdes (v3.14.0) with default settings.[80] Then contigs longer than 1kbp were pooled from all samples, and redundant contigs were filtered using dedupe.sh. Afterward, viral contigs were predicted with the combination of VirSorter (v1.0.6)[81], CAT (v5.0.4)[82], and DeepVirFinder(v1.0)[83]. The viral contigs were clustered by CD-HIT[84]; viral contigs that shared more than 95% identity over 80% of the contig length were considered identical and the longest viral contigs in each cluster were used as representative viral contigs for further analysis.

Virome data analysis

Viral richness (Ace), diversity (Effective Shannon Index) and Principal Coordinates Analysis (PCoA) based on “Bray-Curtis” similarities were conducted in R (Version 3.2, package vegan). The significant difference was determined by Permutational Multivariate Analysis of Variance (PERMANOVA). Means of groups were compared with the Wilcoxon Rank Sum test (two-sided) adjusted for multiple comparisons with the Bonferroni method. The corr.test function in Psych R package v2.1.9 was used to compute the Pearson correlation and multiple comparisons were corrected using Holm method (alpha=0.05). Graphs were generated in Prism 9 (GraphPad), Origin 2020b, Microsoft Excel, and R (Version 3.3.3, ggplot2 package). P-values are shown either as exact value (Figure Legends) or as P-value summary (Figures): ns…not significant (p > 0.05); *…p <0.05; **…p <0.01; ***…p <0.001; ****…p <0.0001.

Metabolome Analysis

Background

Metabolite screening was preceded by a comprehensive testing phase, and we determined that for multi-centric comparisons the use of unprocessed, fresh-frozen native stool samples was essential. Clinical

experience showed us that stool consistency is widely divergent, especially in patients suffering from GI-GvHD with frequent bouts of watery diarrhea. Therefore, we measured metabolite levels in µmol per gram of dry feces to enable cross-sample comparisons regardless of stool consistency. Our methodology was accurate enough to detect reproducible and significant differences in metabolite levels by time-point or diagnosis down to the nmol per gram range.

Sample preparation for targeted analysis

Approximately 100 mg of stool was weighed in a 15 mL bead beater tube (CKMix50 15 mL, Bertin Technologies, Montigny-le-Bretonneux, France) filled with 2.8 mm and 5.0 mm ceramic beads i.d. 5 mL of methanol-based dehydrocholic acid extraction solvent (c=1.3 µmol/L) was added as an internal standard for work-up losses. The samples were extracted with a bead beater (Precellys Evolution, Bertin Technolgies) supplied with a Cryolys cooling module 3 times each for 20 seconds with 15 seconds breaks in between at 10,000 rpm. 1 mL of the fecal suspension was dried in a vacuum centrifuge (Eppendorf Vacufuge) to determine the dry weight.

Targeted short chain fatty acid (SCFA), lactic acid, desaminotyrosine and indole-3-carboxyaldehyde measurement (Panel 1)

The 3-NPH method was used for the quantitation of SCFAs as well as lactic acid, desaminotyrosine and indole-3-carboxyaldehyde[85]. Briefly, 40 µL of the fecal extract and 15 µL of 50 µM isotopically labeled standards were mixed with 20 µL 120 mM EDC HCl-6% pyridine-solution and 20 µL of 200 mM 3-NPH HCL solution. After 30 min at 40°C and shaking at 1000 rpm using an Eppendorf Thermomix (Eppendorf, Hamburg, Germany), 900 µL acetonitrile/water (50/50, v/v) was added. After centrifugation at 13000 U/min for 2 min the clear supernatant was used for analysis. The same system as described above was used. The electrospray voltage was -4500 V, curtain gas 35 psi, ion source gas 1 55 psi, ion source gas 2 65 psi and the temperature 500°C. The MRM-parameters were optimized using commercially available standards. The chromatographic separation was performed on a 1.7 µm, 100 × 2.1 mm, 100 Å Kinetex C18 column (Phenomenex, Aschaffenburg, Germany) column with 0.1% formic acid (eluent A) and 0.1% formic acid in acetonitrile (eluent B) as elution solvents. An injection volume of 1 µL and a flow rate of 0.4 mL/min was used. The gradient elution started at 23% B which was held for 3 min, afterward the concentration was increased to 30% B at 4 min, with another increase to 40%B at 6.5 min, at 7 min 100% B was used which was hold for 1 min, at 8.5 min the column was equilibrated at starting conditions. The column oven was set to 40°C and the autosampler to 15°C. Data acquisition and instrumental control were performed with Analyst 1.7 software (Sciex, Darmstadt, Germany). The data was analyzed with MultiQuant 3.0.3 (Sciex, Darmstadt, Germany) and Metaboanalyst[86]. Features with more than 70% of missing values were removed. Missing values were replaced by LoDs (1/5 of the minimum positive value of each variable). Heatmaps were generated after normalization by log transformation (base 10). Means of multiple groups (time-points) were compared with the Kruskal-Wallis test followed by Dunn's multiple comparisons test. Comparisons between two groups (No ABX versus ABX; No GI-GvHD versus GI-GvHD)

were performed with the Mann-Whitney test (two-sided). Graphs and statistics were created in Prism 8 (GraphPad). P-values are shown either as exact value (Figure Legends) or as P-value summary (Figures): ns…not significant (p > 0.05); *…p <0.05; **…p <0.01; ***…p <0.001; ****…p <0.0001.

Targeted bile acid measurement (Panel 2)

Bile acid analysis was performed according to Reiter et al. 2020[87]. Briefly, 20 µL of isotopically labeled BAs (ca. 7 µM each) were added to 100 µL of fecal extract. Targeted bile acid measurement was performed using a QTRAP 5500 triple quadrupole mass spectrometer (Sciex, Darmstadt, Germany) coupled to an ExionLC AD (Sciex, Darmstadt, Germany) ultrahigh performance liquid chromatography system. A multiple reaction monitoring (MRM) method was used for the detection and quantification of the BAs (Reiter et al., 2020). An electrospray ion voltage of −4500 V and the following ion source parameters were used: curtain gas (35 psi), temperature (450 °C), gas 1 (55 psi), gas 2 (65 psi), and entrance potential (−10 V). The MS parameters and LC conditions were optimized using commercially available standards of endogenous BAs and deuterated BAs, for the simultaneous quantification of selected 34 analytes. For separation of the analytes a 100 × 2.1 mm, 100 Å, 1.7 µm, Kinetex C18 column (Phenomenex, Aschaffenburg, Germany) was used. Chromatographic separation was performed with a constant flow rate of 0.4 mL/min using a mobile phase consisted of water (eluent A) and acetonitrile/water (95/5, v/v, eluent B), both containing 5 mM ammonium acetate and 0.1% formic acid. The gradient elution started with 25% B for 2 min, increased at 3.5 min to 27% B, in 2 min to 35% B, which was hold until 10 min, increased in 1 min to 43% B, held for 1 min, increased in 2 min to 58% B, held 3 min isocratically at 58% B, then the concentration was increased to 65% at 17.5 min, with another increase to 80% B at 18 min, following an increase at 19 min to 100% B which was hold for 1 min, at 20.5 min the column was equilibrated for 4.5 min at starting. The injection volume for all samples was 1 µL, the column oven temperature was set to 40 °C, and the auto-sampler was kept at 15 °C. Data acquisition and instrumental control were performed with Analyst 1.7 software (Sciex, Darmstadt, Germany). The data was analyzed as indicated in Panel 1.

Multi-omics Factor Analysis (MOFA)

MOFA accepts all multi-omics data from the same set of samples, and infers a set of factors that explain sample heterogeneity or variance. Although these factors are derived from all available multi-omics modalities (16S, ITS, virome and metabolomics), the contribution of each omics modality to total variance and each factor can be distinguished.[88]

We opted for an unbiased approach, and decided against inputting clinical and sample meta-data such as diagnosis or time-point for model generation, in order to identify whether factors inferred only from multi-omics data could explain heterogeneity in our study population.

To generate a model by which MOFA could identify factors, we integrated bacterial and fungal ASVs as well as assembled viral contigs at genus level with Panel 1 and Panel 2 metabolite data as published[45]. The input consisted of bacterial 16S rRNA ASVs, fungal ITS1 rRNA ASVs, viral sequences and metabolite concentrations. All inputs were normalized by centralized log normalization (metagenomic data) or log transformation (base 10, metabolomic data). After model fitting, we selected for the top 10 factors with minimum of 1.14% average variance explained across all modalities and with varying degrees of variance explained across the different kingdoms (**Figure 3B**), ordered by total variance explained (i.e., Factor 1 contributed the most, Factor 10 the least to total variation). For each factor, MOFA learns a weight for every feature contributing to that factor, which can be interpreted as a measure of feature importance (**Figure 3D**). Larger weights (approaching 1.0) indicate a higher correlation with that factor, while the positive or negative sign indicates the directionality of that variation (a positive weight represents a positive association and *vice versa*).

Fecal microbiota transplantation

We performed fecal microbiota transplantation (FMT) within compassionate use in accordance to protocols approved by Bavarian authorities. Regulations in Germany allow for the treatment of individuals within compassionate use („individueller Heilversuch“). This requires approval of the local government. We have obtained this approval (General Administration of the Free State of Bavaria, reference number „2677.Ph_3-748-1“, issued to PD Dr. med. Christian Schulz) as well as patient informed consent to treatment and informed consent to publication (according to recommendations by the Committee on Publication Ethics).

FMT was performed as last-line treatment, of severe grade IV GI-GvHD that was refractory to steroids, ruxolitinib and immunosuppressive therapy. The recipient patient (Patient 3, **Supp. Table 4**) received two separate FMTs at Days 0 and +8 from the same healthy, unrelated FMT donor. At Day +13, we were able to discharge the patient in good condition. She is alive and well at the time of writing.

Prior to transplantation, the FMT donor was screened according to site-specific standard operating procedures at the Ludwig-Maximilians University Munich and the University Hospital Regensburg in compliance with regulations issued by the German Federal Institute for Drugs and Medical Devices (**Supp. Table 5**). Of note, SARS-CoV-2 screening was not performed as the FMT occurred before the COVID-19 pandemic. The FMT product consisted of a homogenized suspension of freshly-sampled feces in sterile saline solution and was applied via colonoscopy at the MUC endoscopy suite. During and following the procedure, the patient’s vital signs (ECG, blood pressure, pulse, temperature, peripheral oxygen saturation) were monitored.

The following criteria were used to assess response to FMT:

- CR (complete response) was defined as complete resolution of GI-GvHD.

- VGPR (very good partial response) was defined as improvement of at least 2 stages in the severity of GI-GvHD except improvement to stage 0.
- PR (partial response) was defined as improvement of one stage in the severity of GI GvHD except improvement to stage 0.

Histology

For confirmation of acute GI-GvHD via histopathology, Patient 3 underwent colonoscopy and intestinal biopsies were obtained from the sigma at Day -5 (Before FMT) and Day + 289 (after FMT). Intestinal biopsies were formalin-fixed and embedded in paraffine. Slides were cut with a rotary microtome and stained with hematoxylin-eosin and IHC was performed for CD3 (DCS, clone SP7) and Ki67 (Dako, clone MIB1) (**Supp. Table 6**). The grading of GvHD was performed according to Lerner (1974)[33]. All slides were scanned with a slide scanner (Leica, AT2) and images were acquired using Aperio ImageScope (v. 12.3.1.5011).

ChipCytometry

ChipCytometry of human FFPE biopsies was performed according to the procedure described by Jarosch et al.[89]. Briefly, tissue sections were rehydrated on coverslips and antigen retrieval was performed using TRIS-EDTA buffer (pH 8.5). Sections were then transferred to CellSafe Chips (ZELLKRAFTWERK) and cyclic immunofluorescence with photobleaching was performed on the chip (**Supp. Table 6**).

Declarations

Acknowledgements

This study was supported by Deutsche Forschungsgemeinschaft – Projektnummer 360372040 – SFB 1335 (to S.H., H.P., K.S. and F.B.), Projektnummer 395357507 – SFB 1371 (to H.P., E.T.O., K.P.J., M.Q., K.S. and E.H.), Projektnummer 324392634 – TRR 221 (to H.P. and E.H.), and DFG grant BA 2851/6-1 to F.B, the German Cancer Aid (70114547 to H.P.), the Wilhelm Sander Foundation (2021.040.1 to H.P.), the European Hematology Association (to H.P), The Else- Kröner-Fresenius-Stiftung (funding line: Else-Kröner Forschungskolleg), The Bavarian State Ministry of Science and Art (to H.P.), DKMS Foundation for Giving Life (to H.P), the German José Carreras Leukemia Foundation (grant DJCLS 01 GvHD/2016 to E.H.), the Else-Kröner-Fresenius-Stiftung (fellowship to E. T.O and E.M.), the European Research Commission (project BCM-UPS, Grant No. 682473 to F.B.), the Deutsches Konsortium für Translationale Krebsforschung (fellowship to E. T. O.) and the Deutsche Gesellschaft für Innere Medizin (fellowship to E.T.O.). H. P. is supported by the EMBO Young Investigator Program.

The authors thank the REG allo-SCT team, especially Heike Bremm, Massimiliano Caioni, Tatjana Schifferstein and Yvonne Schumann for their help in collecting and cryopreserving stool samples, and

Sigrun Gleich for data management. The authors express gratitude to the MUC allo-SCT Team, especially Krishan Braitsch, Kathrin Koch, Lena Oßwald, Katharina Nickel, Mareike Verbeek and the entire D2a nursing staff for their excellency in sample acquisition. The authors would like to acknowledge Christian Schulz for providing the FMT product, Anja Conrad and Widya Johannes (Janssen lab) for help with biobanking, Adam Wahida for logistical support as well as the MUC ColoBAC team: Roland Schmid, Plamena Koyumdzhieva, Moritz Middelhoff, Marina Frolova, Julia Horstmann, Lisa Fricke. The authors thank the tissue bank of MRI and TUM (MTBIO) for excellent technical support.

Authorship Contributions

- Conceptualization: E.T.O., H.P.
- Methodology: A.H., J.X., M.G., K.K., S.J., K.S., M.Q.
- Formal analysis: E.T.O., E.M., A.H., J.X.,
- Investigation: E.T.O., E.M., S.Gh., T.E., S.Gö., A.S.
- Resources: C.S., D.Weber, D.Wolff, M.E., W.H., P.H., M.V., F.B., M.Q., K.P.J.
- Data Curation: E.T.O., E.M., M.T.
- Writing - Original Draft: E.T.O., E.M.
- Writing - Review & Editing: E.T.O., E.M., J.F., S.H., L.D., E.H., H.P.
- Visualization: E.T.O., E.M., A.H., J.X., T.E., S.Gö., A.S.
- Supervision: D.B., A.G., L.D., E.H. and H.P.
- Project administration: E.T.O.

Contributions specified according to CRediT (Contributor Roles Taxonomy). All authors read, revised and approved the final draft.

Disclosure of Conflicts of Interest

EH: SAB Maat pharma, Pharmabiome (Novartis/Medac)

HP: honoraria: Novartis, Gilead, Abbvie, BMS; Servier; Travel: Janssen-Cilag, Novartis, Abbvie, Novartis; Research: BMS

References

1. Zeiser R, Blazar BR. Acute Graft-versus-Host Disease — Biologic Process, Prevention, and Therapy. Longo DL, ed. *N Engl J Med*. 2017;377(22):2167–2179. doi:10.1056/NEJMra1609337
2. Holler E, Butzhammer P, Schmid K, et al. Metagenomic analysis of the stool microbiome in patients receiving allogeneic stem cell transplantation: loss of diversity is associated with use of systemic antibiotics and more pronounced in gastrointestinal graft-versus-host disease. *Biol Blood Marrow Transpl*. 2014;20(5):640–645. doi:10.1016/j.bbmt.2014.01.030

3. Taur Y, Xavier JB, Lipuma L, et al. Intestinal Domination and the Risk of Bacteremia in Patients Undergoing Allogeneic Hematopoietic Stem Cell Transplantation. *Clin Infect Dis*. 2012;55(7):905–914. doi:10.1093/cid/cis580
4. Stoma I, Littmann ER, Peled JU, et al. Compositional flux within the intestinal microbiota and risk for bloodstream infection with gram-negative bacteria. *Clin Infect Dis*. Published online January 24, 2020:ciaa068. doi:10.1093/cid/ciaa068
5. Golob JL, Pergam SA, Srinivasan S, et al. Stool Microbiota at Neutrophil Recovery Is Predictive for Severe Acute Graft vs Host Disease After Hematopoietic Cell Transplantation. *Clin Infect Dis*. 2017;65(12):1984–1991. doi:10.1093/cid/cix699
6. Weber D, Hiergeist A, Weber M, et al. Detrimental Effect of Broad-spectrum Antibiotics on Intestinal Microbiome Diversity in Patients After Allogeneic Stem Cell Transplantation: Lack of Commensal Sparing Antibiotics. *Clin Infect Dis*. 2018;68(8):1303–1310. doi:10.1093/cid/ciy711
7. Malard F, Gasc C, Plantamura E, Doré J. High gastrointestinal microbial diversity and clinical outcome in graft-versus-host disease patients. *Bone Marrow Transplant*. 2018;53(12):1493–1497. doi:10.1038/s41409-018-0254-x
8. Peled JU, Gomes ALC, Devlin SM, et al. Microbiota as Predictor of Mortality in Allogeneic Hematopoietic-Cell Transplantation. *N Engl J Med*. 2020;382(9):822–834. doi:10.1056/NEJMoa1900623
9. Shono Y, Docampo MD, Peled JU, et al. Increased GVHD-related mortality with broad-spectrum antibiotic use after allogeneic hematopoietic stem cell transplantation in human patients and mice. *Sci Transl Med*. 2016;8(339):339ra71-339ra71. doi:10.1126/scitranslmed.aaf2311
10. Weber D, Jenq RR, Peled JU, et al. Microbiota Disruption Induced by Early Use of Broad-Spectrum Antibiotics Is an Independent Risk Factor of Outcome after Allogeneic Stem Cell Transplantation. *Biol Blood Marrow Transplant*. 2017;23(5):845–852. doi:10.1016/j.bbmt.2017.02.006
11. Stein-Thoeringer CK, Nichols KB, Lazrak A, et al. Lactose drives Enterococcus expansion to promote graft-versus-host disease. *Science*. 2019;366(6469):1143–1149. doi:10.1126/science.aax3760
12. Jenq RR, Ubeda C, Taur Y, et al. Regulation of intestinal inflammation by microbiota following allogeneic bone marrow transplantation. *J Exp Med*. 2012;209(5):903–911. doi:10.1084/jem.20112408
13. Rolling T, Zhai B, Gjonbalaj M, et al. Haematopoietic cell transplantation outcomes are linked to intestinal mycobiota dynamics and an expansion of Candida parapsilosis complex species. *Nat Microbiol*. 2021;6(12):1505–1515. doi:10.1038/s41564-021-00989-7
14. Zanella MC, Cordey S, Laubscher F, et al. Unmasking viral sequences by metagenomic next-generation sequencing in adult human blood samples during steroid-refractory/dependent graft-versus-host disease. *Microbiome*. 2021;9(1):28. doi:10.1186/s40168-020-00953-3
15. Legoff J, Resche-Rigon M, Bouquet J, et al. The eukaryotic gut virome in hematopoietic stem cell transplantation: new clues in enteric graft-versus-host disease. *Nat Med*. 2017;23(9):1080–1085. doi:10.1038/nm.4380

16. Kim S, Covington A, Pamer EG. The intestinal microbiota: Antibiotics, colonization resistance, and enteric pathogens. *Immunol Rev*. 2017;279(1):90–105. doi:10.1111/imr.12563
17. Mathewson ND, Jenq R, Mathew AV, et al. Gut microbiome–derived metabolites modulate intestinal epithelial cell damage and mitigate graft-versus-host disease. *Nat Immunol*. 2016;17(5):505–513. doi:10.1038/ni.3400
18. Swimm A, Giver CR, DeFilipp Z, et al. Indoles derived from intestinal microbiota act via type I interferon signaling to limit graft-versus-host disease. *Blood*. 2018;132(23):2506–2519. doi:10.1182/blood-2018-03-838193
19. Campbell C, McKenney PT, Konstantinovsky D, et al. Bacterial metabolism of bile acids promotes generation of peripheral regulatory T cells. *Nature*. 2020;581(7809):475–479. doi:10.1038/s41586-020-2193-0
20. Payen M, Nicolis I, Robin M, et al. Functional and phylogenetic alterations in gut microbiome are linked to graft-versus-host disease severity. *Blood Adv*. 2020;4(9):1824–1832. doi:10.1182/bloodadvances.2020001531
21. Yang W, Yu T, Huang X, et al. Intestinal microbiota-derived short-chain fatty acids regulation of immune cell IL-22 production and gut immunity. *Nat Commun*. 2020;11(1):4457. doi:10.1038/s41467-020-18262-6
22. Zelante T, Iannitti RG, Cunha C, et al. Tryptophan Catabolites from Microbiota Engage Aryl Hydrocarbon Receptor and Balance Mucosal Reactivity via Interleukin-22. *Immunity*. 2013;39(2):372–385. doi:10.1016/j.immuni.2013.08.003
23. Bommarius B, Anyanful A, Izrayelit Y, et al. A Family of Indoles Regulate Virulence and Shiga Toxin Production in Pathogenic E. coli. Bereswill S, ed. *PLoS ONE*. 2013;8(1):e54456. doi:10.1371/journal.pone.0054456
24. Martino PD, Fursy R, Bret L, Sundararaju B, Phillips RS. Indole can act as an extracellular signal to regulate biofilm formation of Escherichia coli and other indole-producing bacteria. *Can J Microbiol*. 2003;49(7):443–449. doi:10.1139/w03-056
25. Campbell C, McKenney PT, Konstantinovsky D, et al. Bacterial metabolism of bile acids promotes generation of peripheral regulatory T cells. *Nature*. 2020;581(7809):475–479. doi:10.1038/s41586-020-2193-0
26. Antunes KH, Fachi JL, de Paula R, et al. Microbiota-derived acetate protects against respiratory syncytial virus infection through a GPR43-type 1 interferon response. *Nat Commun*. 2019;10(1):3273. doi:10.1038/s41467-019-11152-6
27. Winkler ES, Shrihari S, Hykes BL, et al. The Intestinal Microbiome Restricts Alphavirus Infection and Dissemination through a Bile Acid-Type I IFN Signaling Axis. *Cell*. 2020;182(4):901–918.e18. doi:10.1016/j.cell.2020.06.029
28. Fischer JC, Bscheider M, Göttert S, et al. Type I interferon signaling before hematopoietic stem cell transplantation lowers donor T cell activation via reduced allogenicity of recipient cells. *Sci Rep*. 2019;9(1):14955. doi:10.1038/s41598-019-51431-2

29. Holmstrøm K, Collins MD, Møller T, Falsen E, Lawson PA. Subdoligranulum variabile gen. nov., sp. nov. from human feces. *Anaerobe*. 2004;10(3):197–203. doi:10.1016/j.anaerobe.2004.01.004
30. Kim JS, Park JE, Lee KC, et al. Blautia faecicola sp. nov., isolated from faeces from a healthy human. *Int J Syst Evol Microbiol*. 2020;70(3):2059–2065. doi:10.1099/ijsem.0.004015
31. Sofi MH, Wu Y, Ticer T, et al. A single strain of Bacteroides fragilis protects gut integrity and reduces GVHD. *JCI Insight*. 2021;6(3):e136841. doi:10.1172/jci.insight.136841
32. Shono Y, Docampo MD, Peled JU, et al. Increased GVHD-related mortality with broad-spectrum antibiotic use after allogeneic hematopoietic stem cell transplantation in human patients and mice. *Sci Transl Med*. 2016;8(339):339ra71-339ra71. doi:10.1126/scitranslmed.aaf2311
33. Lerner KG, Kao GF, Storb R, Buckner CD, Clift RA, Thomas ED. Histopathology of graft-vs.-host reaction (GvHR) in human recipients of marrow from HL-A-matched sibling donors. *Transplant Proc*. 1974;6(4):367–371.
34. Sale GE, Shulman HM, Mcdonald GB, THomas ED. Gastrointestinal graft-versus-host disease in man: A clinicopathologic study of the rectal biopsy. *Am J Surg Pathol*. 1979;3(4):291–300. doi:10.1097/00000478-197908000-00001
35. Elias S, Rudensky AY. Therapeutic use of regulatory T cells for graft-versus-host disease. *Br J Haematol*. 2019;187(1):25–38. doi:10.1111/bjh.16157
36. Lee J, d'Aigle J, Atadja L, et al. Gut Microbiota–Derived Short-Chain Fatty Acids Promote Poststroke Recovery in Aged Mice. *Circ Res*. 2020;127(4):453–465. doi:10.1161/CIRCRESAHA.119.316448
37. Golob JL, DeMeules MM, Loeffelholz T, et al. Butyrogenic bacteria after acute graft-versus-host disease (GVHD) are associated with the development of steroid-refractory GVHD. *Blood Adv*. 2019;3(19):2866–2869. doi:10.1182/bloodadvances.2019000362
38. Stein-Thoeringer CK, Nichols KB, Lazrak A, et al. Lactose drives Enterococcus expansion to promote graft-versus-host disease. *Science*. 2019;366(6469):1143–1149. doi:10.1126/science.aax3760
39. Malard F, Lavelle A, Battipaglia G, et al. Impact of gut fungal and bacterial communities on the outcome of allogeneic hematopoietic cell transplantation. *Mucosal Immunol*. 2021;14(5):1127–1132. doi:10.1038/s41385-021-00429-z
40. Rolling T, Zhai B, Gjonbalaj M, et al. *Intestinal Fungal Dynamics and Linkage to Hematopoietic Cell Transplantation Outcomes*. Hematology; 2021. doi:10.1101/2021.07.20.21260859
41. Uhl FM, Chen S, O'Sullivan D, et al. Metabolic reprogramming of donor T cells enhances graft-versus-leukemia effects in mice and humans. *Sci Transl Med*. 2020;12(567):eabb8969. doi:10.1126/scitranslmed.abb8969
42. van der Lelie D, Oka A, Taghavi S, et al. Rationally designed bacterial consortia to treat chronic immune-mediated colitis and restore intestinal homeostasis. *Nat Commun*. 2021;12(1):3105. doi:10.1038/s41467-021-23460-x
43. Legoff J, Resche-Rigon M, Bouquet J, et al. The eukaryotic gut virome in hematopoietic stem cell transplantation: new clues in enteric graft-versus-host disease. *Nat Med*. 2017;23(9):1080–1085. doi:10.1038/nm.4380

44. Stephen AM, Cummings JH. THE MICROBIAL CONTRIBUTION TO HUMAN FAECAL MASS. *J Med Microbiol*. 1980;13(1):45–56. doi:10.1099/00222615-13-1-45
45. Haak BW, Argelaguet R, Kinsella CM, et al. Integrative Transkingdom Analysis of the Gut Microbiome in Antibiotic Perturbation and Critical Illness. Chia N, ed. *mSystems*. 2021;6(2):e01148-20. doi:10.1128/mSystems.01148-20
46. Fujiwara H, Docampo MD, Riwes M, et al. Microbial metabolite sensor GPR43 controls severity of experimental GVHD. *Nat Commun*. 2018;9(1):3674. doi:10.1038/s41467-018-06048-w
47. Michonneau D, Latis E, Curis E, et al. Metabolomics analysis of human acute graft-versus-host disease reveals changes in host and microbiota-derived metabolites. *Nat Commun*. 2019;10(1):5695. doi:10.1038/s41467-019-13498-3
48. Puccetti M, Pariano M, Borghi M, et al. Enteric formulated indole-3-carboxaldehyde targets the aryl hydrocarbon receptor for protection in a murine model of metabolic syndrome. *Int J Pharm*. 2021;602:120610. doi:10.1016/j.ijpharm.2021.120610
49. Devaux CA, Million M, Raoult D. The Butyrogenic and Lactic Bacteria of the Gut Microbiota Determine the Outcome of Allogenic Hematopoietic Cell Transplant. *Front Microbiol*. 2020;11:1642. doi:10.3389/fmicb.2020.01642
50. Meedt E, Hiergeist A, Gessner A, et al. Prolonged suppression of butyrate producing bacteria is associated with acute gastrointestinal graft-versus-host disease and transplant related mortality after allogeneic stem cell transplantation. *Clin Infect Dis*. Published online May 27, 2021:ciab500. doi:10.1093/cid/ciab500
51. Romick-Rosendale LE, Haslam DB, Lane A, et al. Antibiotic Exposure and Reduced Short Chain Fatty Acid Production after Hematopoietic Stem Cell Transplant. *Biol Blood Marrow Transplant*. 2018;24(12):2418–2424. doi:10.1016/j.bbmt.2018.07.030
52. Weber D, Hiergeist A, Weber M, et al. Detrimental Effect of Broad-spectrum Antibiotics on Intestinal Microbiome Diversity in Patients After Allogeneic Stem Cell Transplantation: Lack of Commensal Sparing Antibiotics. *Clin Infect Dis*. 2018;68(8):1303–1310. doi:10.1093/cid/ciy711
53. Weber D, Jenq RR, Peled JU, et al. Microbiota Disruption Induced by Early Use of Broad-Spectrum Antibiotics Is an Independent Risk Factor of Outcome after Allogeneic Stem Cell Transplantation. *Biol Blood Marrow Transplant*. 2017;23(5):845–852. doi:10.1016/j.bbmt.2017.02.006
54. van Lier YF, Davids M, Haverkate NJE, et al. Donor fecal microbiota transplantation ameliorates intestinal graft-versus-host disease in allogeneic hematopoietic cell transplant recipients. *Sci Transl Med*. 2020;12(556):eaaz8926. doi:10.1126/scitranslmed.aaz8926
55. Qi X, Li X, Zhao Y, et al. Treating Steroid Refractory Intestinal Acute Graft-vs.-Host Disease With Fecal Microbiota Transplantation: A Pilot Study. *Front Immunol*. 2018;9. doi:10.3389/fimmu.2018.02195
56. DeFilipp Z, Peled JU, Li S, et al. Third-party fecal microbiota transplantation following allo-HCT reconstitutes microbiome diversity. *Blood Adv*. 2018;2(7):745–753. doi:10.1182/bloodadvances.2018017731

57. Malard F. MaaT013 as Salvage Therapy in Ruxolitinib Refractory GI-aGVHD Patients (ARES). Accessed March 17, 2022. https://www.clinicaltrials.gov/ct2/show/NCT04769895
58. Kakihana K, Fujioka Y, Suda W, et al. Fecal microbiota transplantation for patients with steroid-resistant acute graft-versus-host disease of the gut. *Blood*. 2016;128(16):2083–2088. doi:10.1182/blood-2016-05-717652
59. Spindelboeck W, Schulz E, Uhl B, et al. Repeated fecal microbiota transplantations attenuate diarrhea and lead to sustained changes in the fecal microbiota in acute, refractory gastrointestinal graft-*versus*-host-disease. *Haematologica*. 2017;102(5):e210-e213. doi:10.3324/haematol.2016.154351
60. Zhang F, Zuo T, Yeoh YK, et al. Longitudinal dynamics of gut bacteriome, mycobiome and virome after fecal microbiota transplantation in graft-versus-host disease. *Nat Commun*. 2021;12(1):65. doi:10.1038/s41467-020-20240-x
61. Miltiadous O, Waters NR, Andrlova H, et al. Early intestinal microbial features are associated with CD4 T cell recovery after allogeneic hematopoietic transplant. *Blood*. Published online January 21, 2022:blood.2021014255. doi:10.1182/blood.2021014255
62. Ma T, Ru J, Xue J, et al. Differences in Gut Virome Related to Barrett Esophagus and Esophageal Adenocarcinoma. *Microorganisms*. 2021;9(8):1701. doi:10.3390/microorganisms9081701
63. on behalf of the EBMT (European Society for Blood and Marrow Transplantation) Transplant Complications Working Party and the "EBMT – NIH (National Institutes of Health) – CIBMTR (Center for International Blood and Marrow Transplant Research) GvHD Task Force," Schoemans HM, Lee SJ, et al. EBMT – NIH – CIBMTR Task Force position statement on standardized terminology & guidance for graft-versus-host disease assessment. *Bone Marrow Transplant*. 2018;53(11):1401–1415. doi:10.1038/s41409-018-0204-7
64. Stämmler F, Gläsner J, Hiergeist A, et al. Adjusting microbiome profiles for differences in microbial load by spike-in bacteria. *Microbiome*. 2016;4(1):28. doi:10.1186/s40168-016-0175-0
65. Usyk M, Zolnik CP, Patel H, Levi MH, Burk RD. Novel ITS1 Fungal Primers for Characterization of the Mycobiome. Mitchell AP, ed. *mSphere*. 2017;2(6). doi:10.1128/mSphere.00488-17
66. Wahida A, Müller M, Hiergeist A, et al. XIAP restrains TNF-driven intestinal inflammation and dysbiosis by promoting innate immune responses of Paneth and dendritic cells. *Sci Immunol*. 2021;6(65):eabf7235. doi:10.1126/sciimmunol.abf7235
67. Vollmer T, Störmer M, Kleesiek K, Dreier J. Evaluation of Novel Broad-Range Real-Time PCR Assay for Rapid Detection of Human Pathogenic Fungi in Various Clinical Specimens. *J Clin Microbiol*. 2008;46(6):1919–1926. doi:10.1128/JCM.02178-07
68. Bolger AM, Lohse M, Usadel B. Trimmomatic: a flexible trimmer for Illumina sequence data. *Bioinformatics*. 2014;30(15):2114–2120. doi:10.1093/bioinformatics/btu170
69. Martin M. Cutadapt removes adapter sequences from high-throughput sequencing reads. *EMBnet.journal*. 2011;17(1):10. doi:10.14806/ej.17.1.200
70. Callahan BJ, Sankaran K, Fukuyama JA, McMurdie PJ, Holmes SP. Bioconductor Workflow for Microbiome Data Analysis: from raw reads to community analyses. *F1000Research*. 2016;5:1492.

doi:10.12688/f1000research.8986.2

71. Murali A, Bhargava A, Wright ES. IDTAXA: a novel approach for accurate taxonomic classification of microbiome sequences. *Microbiome*. 2018;6(1):140. doi:10.1186/s40168-018-0521-5
72. Quast C, Pruesse E, Yilmaz P, et al. The SILVA ribosomal RNA gene database project: improved data processing and web-based tools. *Nucleic Acids Res*. 2012;41(D1):D590-D596. doi:10.1093/nar/gks1219
73. Nilsson RH, Larsson KH, Taylor AFS, et al. The UNITE database for molecular identification of fungi: handling dark taxa and parallel taxonomic classifications. *Nucleic Acids Res*. 2019;47(D1):D259-D264. doi:10.1093/nar/gky1022
74. McMurdie PJ, Holmes S. phyloseq: An R Package for Reproducible Interactive Analysis and Graphics of Microbiome Census Data. Watson M, ed. *PLoS ONE*. 2013;8(4):e61217. doi:10.1371/journal.pone.0061217
75. Jost L. *Entropy and diversity*. *Oikos*. 2006;113(2):363–375. doi:10.1111/j.2006.0030-1299.14714.x
76. Martinez AP. *PairwiseAdonis: Pairwise Multilevel Comparison Using Adonis. R Package Version 0.4.*; 2020.
77. Yang. *Yiluheihei/MicrobiomeMarker: MicrobiomeMarker 0.0.1*. Zenodo; 2020. doi:10.5281/ZENODO.3749415
78. Chen S, Zhou Y, Chen Y, Gu J. fastp: an ultra-fast all-in-one FASTQ preprocessor. *Bioinformatics*. 2018;34(17):i884-i890. doi:10.1093/bioinformatics/bty560
79. Bushnell, B. BBMap: A Fast, Accurate, Splice-Aware Aligner. In: *Lawrence Berkeley National Lab. (LBNL).*; 2014. https://www.osti.gov/biblio/1241166
80. Nurk S, Meleshko D, Korobeynikov A, Pevzner PA. metaSPAdes: a new versatile metagenomic assembler. *Genome Res*. 2017;27(5):824–834. doi:10.1101/gr.213959.116
81. Roux S, Enault F, Hurwitz BL, Sullivan MB. VirSorter: mining viral signal from microbial genomic data. *PeerJ*. 2015;3:e985. doi:10.7717/peerj.985
82. von Meijenfeldt FAB, Arkhipova K, Cambuy DD, Coutinho FH, Dutilh BE. Robust taxonomic classification of uncharted microbial sequences and bins with CAT and BAT. *Genome Biol*. 2019;20(1):217. doi:10.1186/s13059-019-1817-x
83. Ren J, Song K, Deng C, et al. Identifying viruses from metagenomic data using deep learning. *Quant Biol*. 2020;8(1):64–77. doi:10.1007/s40484-019-0187-4
84. Fu L, Niu B, Zhu Z, Wu S, Li W. CD-HIT: accelerated for clustering the next-generation sequencing data. *Bioinformatics*. 2012;28(23):3150–3152. doi:10.1093/bioinformatics/bts565
85. Weiss AS, Burrichter AG, Durai Raj AC, et al. In vitro interaction network of a synthetic gut bacterial community. *ISME J*. Published online December 2, 2021. doi:10.1038/s41396-021-01153-z
86. Pang Z, Chong J, Zhou G, et al. MetaboAnalyst 5.0: narrowing the gap between raw spectra and functional insights. *Nucleic Acids Res*. 2021;49(W1):W388-W396. doi:10.1093/nar/gkab382

87. Reiter S, Dunkel A, Metwaly A, et al. Development of a Highly Sensitive Ultra-High-Performance Liquid Chromatography Coupled to Electrospray Ionization Tandem Mass Spectrometry Quantitation Method for Fecal Bile Acids and Application on Crohn's Disease Studies. *J Agric Food Chem*. 2021;69(17):5238–5251. doi:10.1021/acs.jafc.1c00769
88. Argelaguet R, Velten B, Arnol D, et al. Multi-Omics Factor Analysis—a framework for unsupervised integration of multi-omics data sets. *Mol Syst Biol*. 2018;14(6). doi:10.15252/msb.20178124
89. Jarosch S, Köhlen J, Sarker RSJ, et al. Multiplexed imaging and automated signal quantification in formalin-fixed paraffin-embedded tissues by ChipCytometry. *Cell Rep Methods*. 2021;1(7):100104. doi:10.1016/j.crmeth.2021.100104

Figures

a

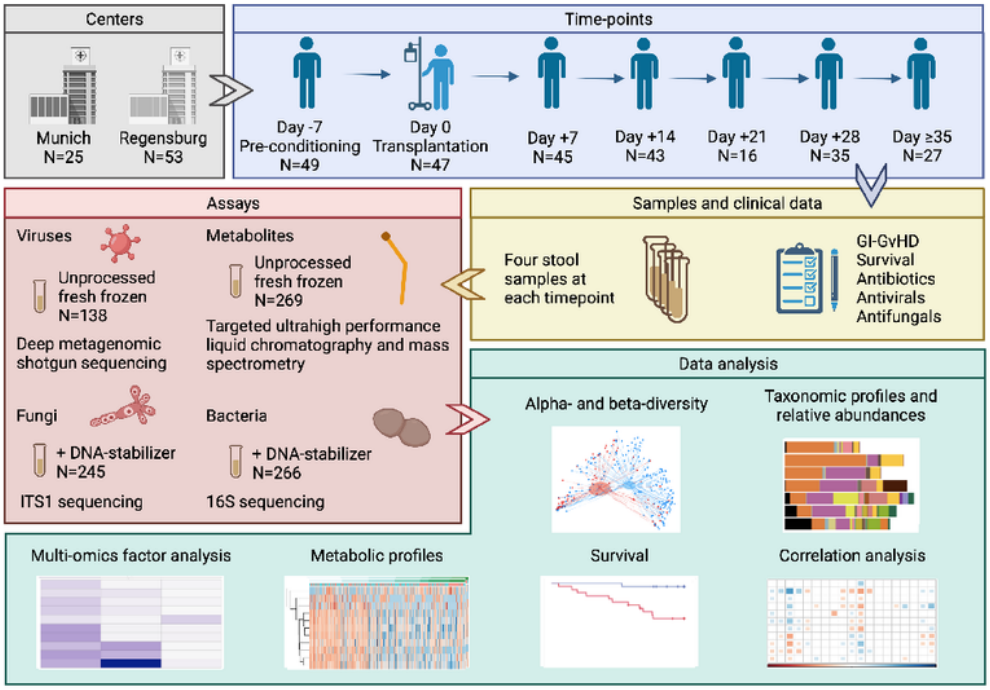

b

		Munich	Regensburg
Patients - no.		25	53
Mean age at HSCT – yrs.		57.4 ± 8.6	54.2 ± 12.2
Male Sex - no. (%)		14 (56)	31 (59)
Diagnosis - no. (%)	Acute leukaemia	10 (40)	28 (53)
	MDS/MPN	9 (36)	15 (28)
	NHL	4 (16)	7 (13)
	other	2 (8)	3 (6)
Donor type - no. (%)	Unrelated	18 (72)	39 (74)
	Sibling	2 (8)	7 (13)
	Haploidentical	5 (20)	7 (13)
Conditioning - no. (%)	Ablative	3 (12)	7 (13)
	Reduced intensity	22 (88)	46 (87)
Stem cell source - no. (%)	PBSC	24 (96)	40 (75)
	BM	1 (4)	13 (25)
GI-GvHD - no. (%)	none	11 (44)	25 (47)
	Mild	3 (12)	18 (34)
	Severe	11 (44)	10 (19)
	Steroid refractory	13 (52)	11 (21)
Relapse - no. (%)		2 (8)	6 (11)
1 year survival - no. (%)		16 (64)	47 (89)

Figure 1

Figure 1

Study design, sampling scheme and patient characteristics

a) Illustration of patient numbers per center, sampling time-points, sampling scheme including processing and storage, sample numbers per multi-omics modality, and downstream analytics. Created with BioRender.

b) Patient characteristics according to transplantation center. A total of 68% of the patients in the overall study population were enrolled at University Medical Center, Regensburg (REG) and 32% at University Hospital Rechts der Isar, Munich (MUC). HSCT denotes hematopoietic stem cell transplantation, MDS myelodysplastic syndrome, MPN myeloproliferative neoplasia, NHL Non-Hodgkin lymphoma, PBSC peripheral-blood stem cell, BM bone marrow and GI-GvHD acute gastrointestinal graft-versus-host disease. Diseases categorized as "other" include aplastic anemia, chronic active Epstein-Barr virus infection, blastic plasmacytoid dendritic cell neoplasm and myelosarcoma.

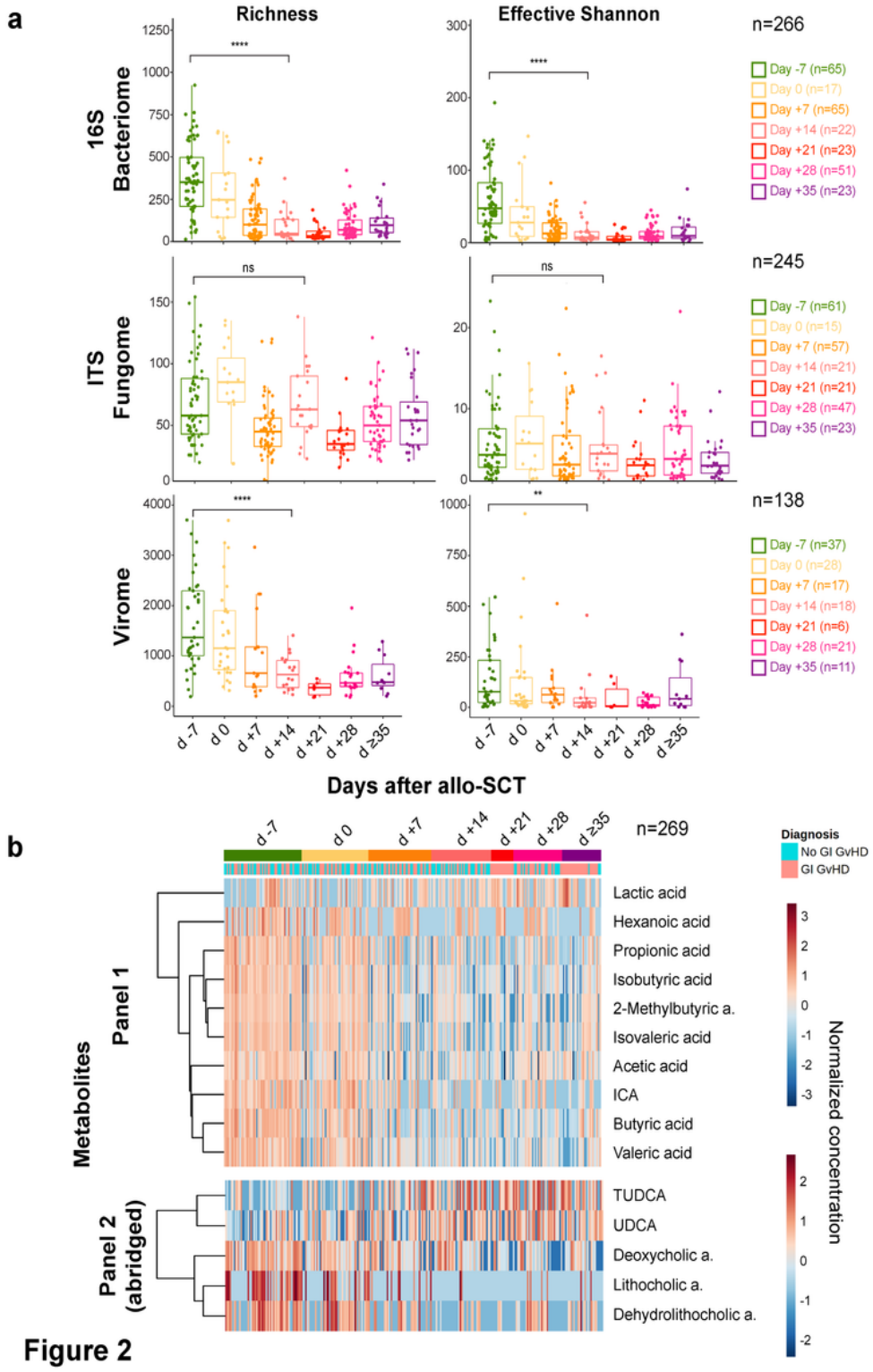

Figure 2

Figure 2

Longitudinal dynamics of intestinal bacteriome, fungome, virome and metabolome before and after allo-SCT

a) Intestinal microbiome composition in bacteriome (16S amplicon sequencing, n=266, $p=4.12*10^{-7}$ and $p=1.01*10^{-5}$), fungome (ITS amplicon sequencing, n=245, ns…not significant) and virome (metagenomic shotgun sequencing, n=138, $p=8.8*10^{-6}$ and p=0.0069) at time-points relative to allo-SCT (Day 0) by alpha diversity (Richness by number of observed Amplicon Sequence Variants (ASVs) and Effective Shannon diversity index, respectively). Significance is shown for Day +14 compared to Day -7 (baseline) by nonparametric two-tailed Wilcoxon rank sum test corrected for multiple comparisons. In the box plots, the box extends from the 25th to 75th percentiles. The line in the middle of the box is plotted at the mean. The whiskers are drawn down to the 10th and up to the 90th percentile. Each individual patient stool sample is plotted as a point superimposed on the graph.

b) Heatmap of metabolite concentration normalized by log transformation (base 10) in stool samples (n=269) of allo-SCT patients ordered by time-points relative to allo-SCT (Day 0). Panel 1 displays short-chain fatty acids (SCFA) including acetate, butyrate, propionate and valeric acid as well as type I-interferon inducing metabolites (IIMs), i.e., indole-3-carboxylaldehyde (ICA) and lactic acid. Panel 2 (abridged) shows selected bile acids (see **Supp. Fig. 2A** for full panel). Diagnosis indicates patients who suffered from gastrointestinal acute GvHD of any severity (GI-GvHD) at any time after allo-SCT or control allo-SCT patients (no GI-GvHD), i.e., if a patient developed GI-GvHD at Day +30, corresponding samples are indicated by light red bars. Clustering based on metabolite expression patterns using the Ward algorithm. Distance measure is Euclidian.

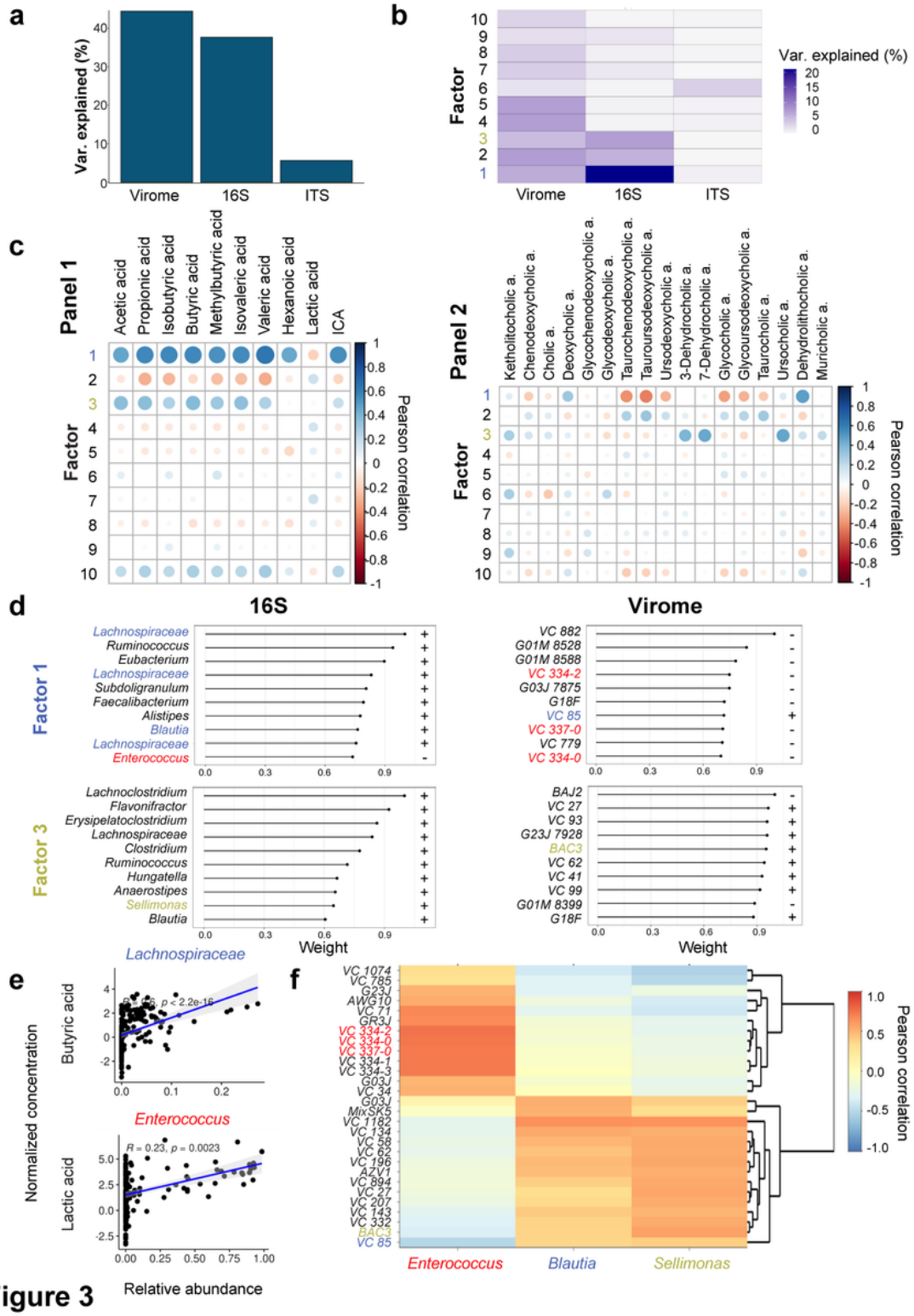

Figure 3

Figure 3

Multi-omics factor analysis (MOFA) of intestinal bacteriome, fungome, virome and metabolome

a) Bar plot of the total variance explained by each kingdom. Viral and bacterial composition contributed most to total variance of data across all patient samples. We employed the MOFA algorithm as previously published[88].

b) MOFA describes major sources of variability in data as factors. The heatmap illustrates the variance explained by each MOFA-identified factor (rows) and the relative contribution of each kingdom to that Factor (columns).

c) Correlation between MOFA-identified Factors and Panel 1 (left panel) as well as Panel 2 (right panel) intestinal metabolite concentrations. Associations between factor values and metabolites were analyzed using linear regression by Pearson correlation coefficients.

d) For each factor (i.e. each major source of variation), MOFA learns a “weight” as a measure of importance of every feature contained within that factor hence enabling the interpretation of the variation captured by that factor[45]. Weights can be interpreted as a measure of feature importance: Larger weights indicate a higher correlation with that factor, while the positive or negative sign indicates the directionality of that variation, i.e., “+” indicates a positive association, “-“ a negative association. Shown is the characterization of top 10 weights in Factors 1 (top panel) and 3 (bottom panel) in bacteriome and virome. Weight values are scaled between 0 and 1. Viral taxa are listed by viral cluster name.

e) Selected correlation plots of bacterial taxa at genus level and metabolites across all samples. Abundance of *Lachnospiraceae* correlate with expression of butyric acid ($R=0.6$, $p<2.2*10^{-16}$) and *Enterococcus* with lactic acid ($R=0.23$, $p=0.0023$). Associations between relative abundance of bacterial taxa and normalized metabolite concentrations were analyzed using linear regression by Pearson correlation coefficients. See **Supp. Figure 3B** for further significant correlations. The R- and p-values are indicated in each plot. The regression line is drawn in blue and 95 % confidence intervals are shaded in grey.

f) Correlation between selected bacterial and viral taxa at genus level across all samples (see **Supp. Figure 3C** for all bacterial/viral correlations). Viral taxa are listed by viral cluster name. Associations between bacterial and viral taxa were analyzed using linear regression by Pearson correlation coefficients. Only significant correlations with a Pearson correlation coefficient above 0.5 are shown. Blue or green font coloring indicates positive co-variation with Factor 1 or Factor 3, respectively, while red coloring indicates negative co-variation with Factor 1 (see **Figure 3D**). The same colors were used to highlight specific bacteria and bacteriophages that were associated with Factors 1 or 3: The bacteriophage viral contig 85 (*VC85)*, the only positively correlated viral taxa in Factor 1, was highly correlated with *Blautia,* a top bacterial weight in Factor 1. *BAC3* was one of the top viral weights in Factor 3, which also contained *Blautia* and *Sellimonas. VC334-2*, one of the top viral weights negatively correlated with Factor 1, was correlated with *Enterococcus,* the only bacterial taxa negatively correlated with Factor 1.

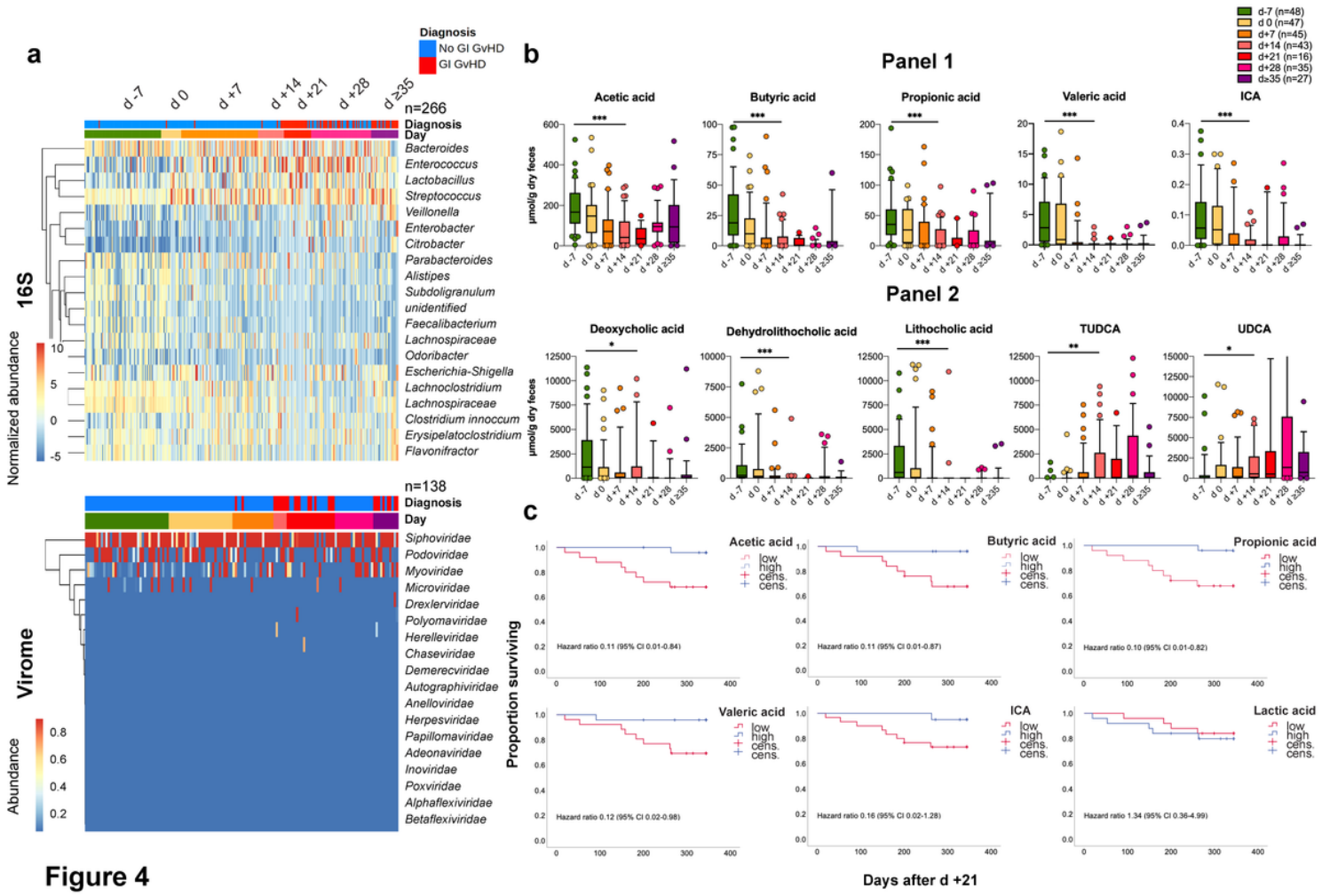

Figure 4

Figure 4

Disruption of bacterial and viral communities after allo-SCT impacts bacterial consortia and their production of protective metabolites

a) Heatmap of normalized abundance of bacterial taxa at genus level (top) and relative abundance of viral taxa at family level (bottom) at time-points relative to allo-SCT (Day 0). Diagnosis indicates GI-GvHD of any severity (red) versus control allo-SCT patients (blue). Number of samples are indicated.

b) Levels of microbiota-derived metabolites at time-points relative to allo-SCT (Day 0) in µmol per gram of dried stool samples measured by targeted mass spectrometry. Metabolites correlated with MOFA Factors 1 and 3 are shown. Top panel displays Panel 1, including SCFA and IIM. Bottom panel displays Panel 2, consisting of BA. Number of samples per time-point are indicated (top right). Significance is shown for Day +14 compared to Day -7 (baseline) by non-parametric two-tailed Kruskal-Wallis test corrected for multiple comparisons (Panel 1: ***…p<0.001; Panel 2: deoxycholic acid p=0.02, dehydrolithocholic acid p<0.001, lithocholic acid p<0.001, TUDCA p=0.001, UDCA p=0.03).

In the box plots, the box extends from the 25th to 75th percentiles. The line in the middle of the box is plotted at the median. The whiskers are drawn down to the 10th and up to the 90th percentile. Points

below and above the whiskers are drawn as individual points. Points indicate individual patient stool samples sampled at specific time-points.

c) Overall survival after Day 21 stratified according to high and low intestinal levels of the metabolites specified in the legend. Patients were stratified into high and low metabolite levels according to the center-specific median intestinal metabolite concentration observed between Days +7 and +21. When a patient had more than one sample in this time frame, the mean value was used for analysis. For acetate, butyrate and propionate, there were 8 deaths among 25 patients in the low group, versus one death among 25 patients in the high group, respectively. For valerate, there were 8 deaths among 26 patients in the low group, contrary to one death among 24 patients in the high group. Accordingly, there were 8 deaths among 30 patients in the ICA-low group in opposition to one death among 20 patients in the ICA-high group. For lactic acid, there were 4 deaths among 25 patients in the low group and 5 deaths among 25 patients in the high group. Analysis by Cox Regression, CI denotes confidence interval.

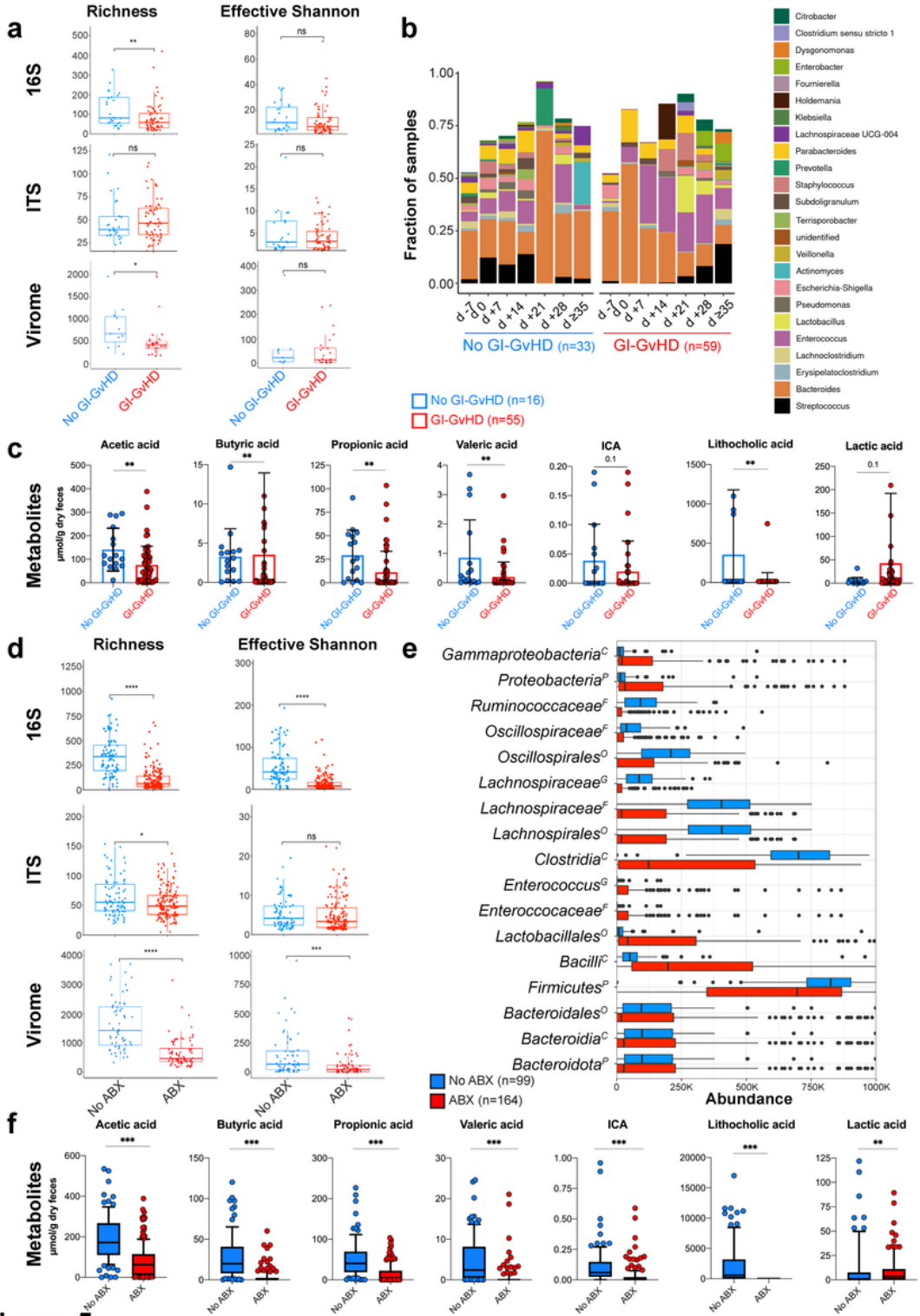

Figure 5

Figure 5

GI-GvHD and antibiotics suppress protective bacterial consortia and their bacteriophages and deplete protective metabolites

a) Intestinal bacterial, fungal and viral alpha diversity (Richness, Effective Shannon diversity index) stratified by patients diagnosed with GI-GvHD (GI-GvHD) versus control allo-SCT patients (No GI-GvHD).

Significance by two-tailed Wilcoxon rank sum test (16S: p=0.00403 and p=0.0895; ITS: ns…not significant; virome: p=0.021 and p=0.93 for Richness and Effective Shannon, respectively). Number of samples: for 16S and ITS n=33 versus n=59; for virome n=11 versus n=26, corresponding to No GI-GvHD versus GI-GvHD, respectively. In the box plots, the box extends from the 25th to 75th percentiles. The line in the middle of the box is plotted at the mean. The whiskers are drawn down to the 10th and up to the 90th percentile. Each individual patient stool sample is plotted as a point superimposed on the graph.

b) Domination by most abundant bacterial taxa by time-points in patients that developed GI-GvHD (n=59) versus control allo-SCT (n=33) patients. Domination was defined as presence of taxa with relative abundance > 50 percent at genus level. Once domination criteria applied a sample was declared positive, fraction of positive samples at each time-point is shown.

c) Levels of selected microbiota-derived metabolites stratified by patients diagnosed with GI-GvHD versus control allo-SCT patients (No GI-GvHD). Significance by nonparametric two-tailed Mann-Whitney test (acetic acid p=0.004, butyric acid p=0.002, propionic acid p=0.003, valeric acid p=0.004, ICA p=0.10, lithocholic acid p=0.003, lactic acid p=0.10). Number of samples per group are indicated above. In the scatter-dot plots, the box is plotted at the mean. Error bars indicate standard deviation. Each individual patient stool sample is plotted as a point superimposed on the graph. For butyric acid, two outliers in the GI-GvHD group resulted in a positive skew, such that the mean (4.23 versus 3.28) was greater than the median (0.11 versus 2.92) for GI-GvHD versus No GI-GvHD, respectively. However, the median expression of butyrate in control allo-SCT patients was significantly higher compared GI-GvHD patients.

d) Intestinal bacterial, fungal and viral diversity alpha diversity (Richness, Effective Shannon diversity index) in patient samples according to antibiotic status: “No Antibiotics (No ABX)” (blue) or “Antibiotics (ABX)” (red). Once a patient was treated with antibiotics, the current and all subsequent samples were classified as “ABX”. Significance by two-tailed Wilcoxon rank sum test (16S: $p=1.16*10^{-23}$ and $p=3.00*10^{-23}$; ITS: p=0.0305 and p=0.229; virome: $p=6*10^{-13}$ and p=0.00013 for Richness and Effective Shannon, respectively). Number of samples: for 16S n=88 versus n=178, for ITS n=82 versus n=163, for virome n=60 versus n=76; corresponding to No ABX versus ABX, respectively. In the box plots, the box extends from the 25th to 75th percentiles. The line in the middle of the box is plotted at the mean. The whiskers are drawn down to the 10th and up to the 90th percentile. Each individual patient stool sample is plotted as a point superimposed on the graph.

e) Impact of systemic antibiotics on bacterial taxa shown as abundance plot. Shown are the most differentially abundant taxa in patient samples according to antibiotic status. Only significantly different taxa are shown (p=0.01 or below). Values in thousands (K). In the box plots, the box extends from the 25th to 75th percentiles, the line is plotted at the mean. The whiskers are drawn down to the 10th and up to the 90th percentile. Points below and above the whiskers are drawn as individual points. Points indicate individual patient stool samples sampled at specific time-points. Text superscript indicates class (C), phylum (P), family (F), order (O) or genus (G).

f) Intestinal metabolite levels in patient samples according to antibiotic status as in d) in µmol per gram of dry stool. Significance by nonparametric two-tailed Mann-Whitney test (*** indicates p<0.001 for acetic acid, butyric acid, propionic acid, valeric acid, ICA and lithocholic acid, whereas for lactic acid ** indicates p=0.002). Box extends from the 25th to 75th percentiles, the line is plotted at the median. Number of samples per group are indicated above. Whiskers from 10th to 90th percentile. Points below and above the whiskers are drawn as individual points. Points indicate individual patient stool samples sampled at specific time-points. In contrast to the other metabolites, the mean expression of lactic acid was significantly higher in ABX-treated patients versus those that did not receive antibiotics (mean 23.43 versus 13.99).

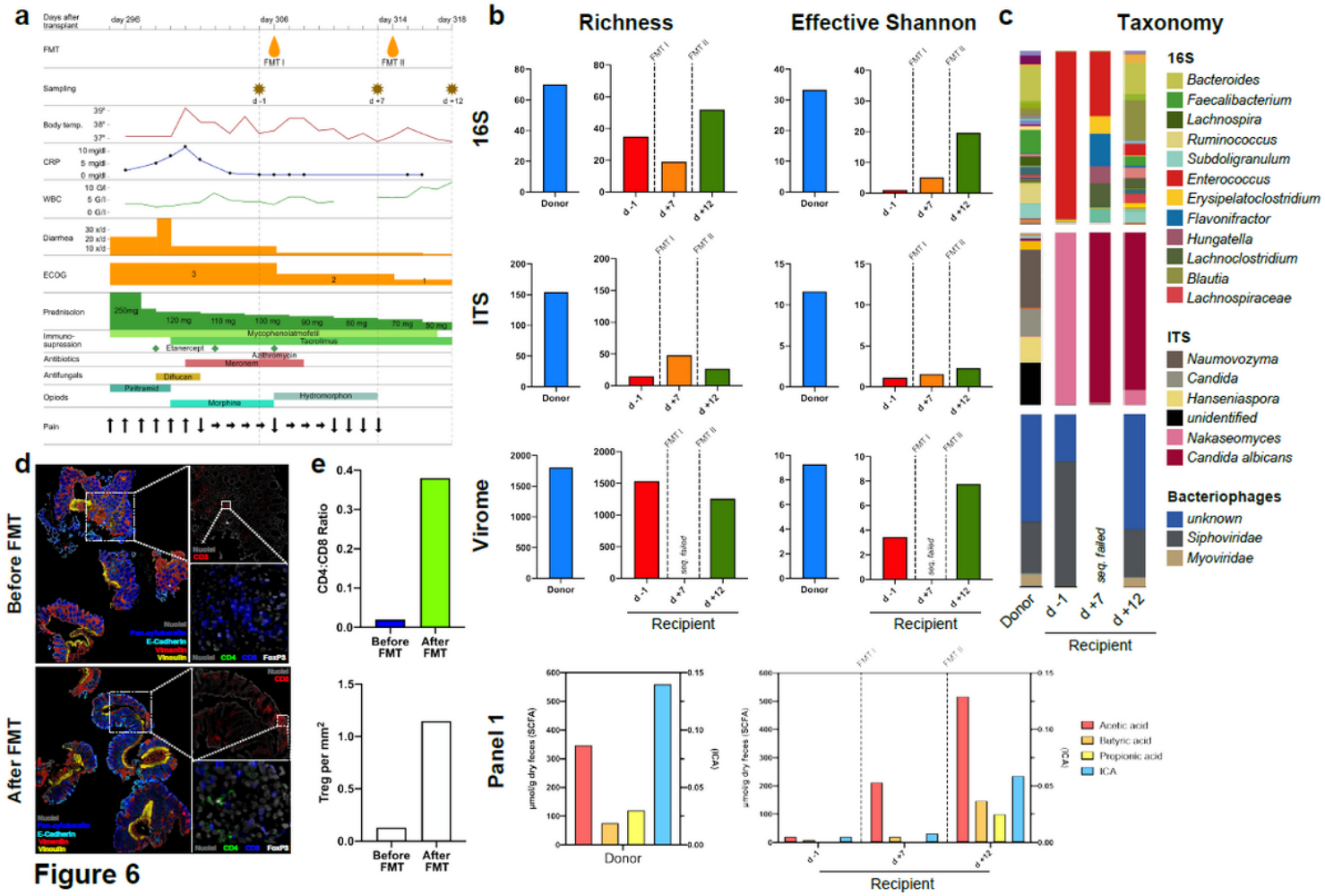

Figure 6

Fecal microbiota transplantation in steroid-refractory GI-GvHD restores intestinal bacterial and viral diversity, protective metabolite expression and tissue homeostasis

a) Clinical vignette of Patient 3 who suffered from severe (clinical grade IV), steroid and ruxolitinib refractory GI-GvHD and received a fecal microbiota transplantation (FMT) as last-line treatment. The clinical course before and after FMT is shown by vital signs, blood counts, anti-infective and immunosuppressive therapy as well as pain medication. FMT was performed on Day 0 and Day 8 (Days

306 and 314 after allo-SCT, respectively). Dotted lines indicate stool sampling time-points for multi-omics analysis (Day -1, Day +7, Day +12 relative to FMT).

b) Top: Profiling changes in intestinal bacteriome, fungome and virome composition by alpha diversity (Richness and Effective Shannon diversity index). The left panel illustrates the FMT donor (“Donor”) sampled at baseline, the right panel Patient 3 (“Recipient”) sampled at the specified time-points relative to FMT. The first (FMT I) and second FMT (FMT II) are indicated by dotted lines. Seq. failed indicates that viral metagenomic sequencing failed due to technical reasons and the data is not available.

Bottom: Profiling changes in intestinal metabolome (Panel 1) at the time-points specified above. SCFA are plotted on the left axis, ICA is plotted on the right axis. Metabolite concentration is shown as µmol per gram dried stool. The box plot indicates the individual value of a stool sample obtained at the respective time-point.

c) Transkingdom taxonomic composition of donor and recipient at the specified time-points relative to FMT. Bacterial and fungal taxonomy are shown at genus level. Viral taxonomy is shown at family level.

d) ChipCytometry of colon biopsy samples obtained before FMT at Day -5 (confirmation of clinical GvHD by histopathology) and after FMT at Day +296 (routine follow-up). Epithelial markers: Pan-cytokeratin, E-cadherin, Vimentin, Vinculin. Lymphocytic markers: CD3, CD4, CD8, Foxp3 (**Supp. Table 6**).

e) Quantification of lymphocytic immune infiltrates in ChipCytometry images. Top panel: CD4:CD8 effector T cell ratio. Bar coloring indicate excess of cytotoxic $CD8^+$ (blue) and $CD4^+$ (green) T cells. Bottom panel: Absolute number of $Foxp3^+$ T regulatory cells per mm^2.

Supplementary Files

This is a list of supplementary files associated with this preprint. Click to download.

- OrbergSupplementalfigures.pdf
- OrbergSupplementalTablesv2.pdf
- flatOrbergepc.pdf
- flatOrbergrs.pdf